

Exact solution of the $2d$ dimer model: Corner free energy, correlation functions and combinatorics

Nicolas Allegra

Groupe de Physique Statistique, IJL, CNRS/UMR 7198, Université de Lorraine

Abstract

In this work, some classical results of the pfaffian theory of the dimer model based on the work of Kasteleyn, Fisher and Temperley are introduced in a fermionic framework. Then we shall detail the bosonic formulation of the model *via* the so-called height mapping and the nature of boundary conditions is unravelled. The complete and detailed fermionic solution of the dimer model on the square lattice with an arbitrary number of monomers is presented, and finite size effect analysis is performed to study surface and corner effects, leading to the extrapolation of the central charge of the model. The solution allows for exact calculations of monomer and dimer correlation functions in the discrete level and the scaling behavior can be inferred in order to find the set of scaling dimensions and compare to the bosonic theory which predict particular features concerning corner behaviors. Finally, some combinatorial and numerical properties of partition functions with boundary monomers are discussed, proved and checked with enumeration algorithms.

URL: `nicolas.allegra@univ-lorraine.fr` (Nicolas Allegra)

¹BP 70239, F-54506 Vandœuvre-lès-Nancy Cedex, France

Contents

1	Introduction	3
2	Kasteleyn solution and bosonic formulation of the dimer model	5
2.1	Dimer model and nilpotent variables	5
2.2	Haffnian to Pfaffian conversion and Kasteleyn solution	7
2.2.1	Entropy in the thermodynamic limit	9
2.2.2	Probabilities and correlations	9
2.3	Monomer correlation functions	10
2.4	Mapping to a bosonic theory	11
2.4.1	Height mapping and Coulomb gas formalism	11
2.4.2	Rectangular geometry and boundary conditions	13
3	Exact partition function and corner free energy	14
3.1	Pleckho pfaffian solution	14
3.2	Pfaffian solution with $2n$ monomers.	16
3.2.1	General case	16
3.2.2	Boundary monomers	20
3.2.3	Single monomer on the boundary	21
3.3	Corner free energy and the central charge controversy	23
4	Exact correlations: discrete and continuous cases	26
4.1	Fermion correlations and disorder operators	27
4.2	Perturbative expansion of the 2-point function	27
4.3	Scaling behavior of monomer correlation functions	29
4.4	Scaling behavior of dimer correlation functions	32
5	About some combinatorial properties	33
5.1	Partition function without monomers	34
5.2	Partition function with two boundary monomers	34
5.2.1	Inline boundary monomers	35
5.2.2	General case	36
5.3	Partition function with $2n$ boundary monomers	37
6	Conclusion	37
	Appendices	39
A	Grassmann variables, determinant permanent and all that	39

1. Introduction

Following Onsager’s solution of the $2d$ Ising model in the forties [114, 81, 82], the introduction of the Bethe ansatz [13] and the discovery of the machinery of transfer matrices, the field of exact solutions of lattice statistical physics models has exploded leading to the birth of a new domain of theoretical and mathematical physics known as *exactly solved models* [10]. The confluence of this new field with $2d$ conformal field theory (CFT) [11] discovered by Belavin, Polyakov and Zamolodchikov (see [35] for an extensive monography) had a huge impact in theoretical physics, from high energy to condensed matter, leading to a whole new level of understanding of classical and quantum integrable systems [98].

Initially, the dimer model (see Fig. 1) has been introduced by physicists to describe absorption of diatomic molecules on a $2d$ substrate [49], yet it became quickly a general problem studied in various scientific communities. From the mathematical point of view, this problem known as perfect matching problem [106]—is a famous and active problem of combinatorics and graph theory [47] with a large spectrum of applications. The enumeration of so-called Kekulé structures of molecular graphs in quantum chemistry are equivalent to the problem of enumeration of perfect matchings [138, 139]. Besides, a recent connection between dimer models and D -brane gauge theories has been discovered [54, 52], providing a very powerful computational tool.

The partition function of the $2d$ dimer model on the square lattice was solved independently using pfaffian methods [79, 41, 135] for several boundary conditions, resulting in the exact calculation of correlation functions of two monomers along a row [43] or along a diagonal [55, 42] in the scaling limit using Toeplitz determinants. For the general case of an arbitrary orientation, exact results are given in terms of the spin correlations of the $2d$ square lattice Ising model at the critical point [6, 94]. Other lattice geometries have been studied as well, *e.g.* the triangular lattice [39], the Kagomé lattice [140, 141, 146], the triangular Kagomé lattice [105], the hexagonal lattice [38], the star lattice [44], or more complicated geometries [147] (see [143] for a review). The case of surface of high genus have been studied as well in [32].

The detailed study of the free energy and finite size effects began with the work of Ferdinand [40] few years after the exact solution, and has continued in a long series of articles using analytical [72, 70, 71, 68, 113] and numerical methods [96, 97, 95, 145] for various geometries and boundary conditions. Some of these results have been motivated by the conformal interpretation of finite size effects [15, 25, 24] and leading to a somehow controversial result [95, 125] about the central charge of the underlying field theory.

Recent advances concern the analytic solution of the problem with a single monomer on the boundary of a $2d$ lattice [136, 144] thanks to a bijection due to Temperley [134], boundary monomer correlation functions [123] and monomer localization phenomena [19, 75, 120]. Dimer models have regained interest because of its quantum version, the so-called quantum dimer model, originally introduced by Rokhsar and Kivelson [127] in a condensed matter context (see [109, 50] for reviews) and equal to the classical model in a specific point of the parameter space. In this context, interactions between dimers have been considered at the classical and quantum level [4, 3, 115, 33], leading to a richer phase diagram.

For the general monomer-dimer problem (*cf.* Appendix C for a definition) there is no exact solution except in $1d$, on the complete and locally tree-like graphs [2] or scale free networks [148]. We can also mention that the matrix transfer method was used to express the partition function of the model [104, 91] and a very efficient method based on variational corner transfer matrix has been found by Baxter [8], leading to precise approximations of thermodynamic quantities of the model. From a more mathematical point of view, many results exist, one can mention the location of the zeros of the partition function [58, 59], series expansions of the

partition function [110] and exact recursion relations [1]. Very recently a integrable version of the monomer-dimer model called monopole-dimer model has been proposed [7], sharing some qualitative features with the genuine monomer-dimer model. For $d > 2$ lattices, no exact solution exists for the dimer model in general, but some analytical [126, 34] and numerical approaches [14, 63] has been performed to study the phase diagram of the model. This lack of exact solution has been formalized in the context of computer science [76].

The prominence of the dimer model in theoretical physics and combinatorics also comes from the direct mapping between the square lattice Ising model without magnetic field and the dimer model on a decorated lattice [108, 79, 41, 135] and conversely from the mapping of the square lattice dimer model to a eight-vertex model [9, 142]. Furthermore the magnetic field Ising model can be mapped onto the general monomer-dimer model [59]. Recently, some properties of the dimer model has been proved rigorously [84, 85, 86] and various correlation functions has been studied as well [26, 27, 36]. We could also mention the study of the double dimer model [88, 87] and the arctic circle phenomena [37, 31] in the Aztec geometry dimer model.

Grassmann variables [12], thanks to their nilpotent properties, are very suitable to tackle combinatorial lattice models, and many of this models has been partially or entirely solved in the frame of fermionic field theory and the dimer model was one of them [128, 129]. In this context, we should mention the study of spanning trees and spanning forests [22, 21] as well as the edge-coloring problem [45, 46] which is a special case of a more general loop model [74, 93]. The approach introduce presently has been developed by Plechko in a series of papers and has been widely used to solve in a very simple and elegant fashion many problems, *e.g.* the $2d$ Ising model [118, 119], boundary-field Ising model [28], the Blume-Capel model [117, 30] or more general spin models [48, 29].

Recently a work based on this approach has been published extending the computation of the partition function of the dimer model with an arbitrary number of monomers [5]. In this present article, we continue the analysis of this solution focusing on the effect of surfaces and corners on the free energy and correlation functions. After reviewing the classical pfaffian theory and some of its most important features in a fermionic formulation, the bosonic version of the dimer model is introduced in order to compare CFT predictions with exact calculations. A special attention will be paid to the influence of boundary conditions to the expression of the free energy and critical exponents. At the end of the article, the exact expression of monomer correlations will be employed to bring out numerical identities about the partition function of the model with boundary monomers.

Acknowledgement

I am grateful to Jean-Yves Fortin for his early collaboration on this project and daily discussions. I would like to thank Jean-Marie Stéphan for crucial help and remarks on the height mapping and Christophe Chatelain, Jérôme Dubail, Malte Henkel, Jesper Jacobsen, Shahin Rouhani and Loïc Turban for insightful discussions and useful comments at different stages of the elaboration of this article. This work was partly supported by the Collège Doctoral Leipzig-Nancy-Coventry-Lviv (Statistical Physics of Complex Systems) of UFA-DFH.

2. Kasteleyn solution and bosonic formulation of the dimer model

In this section, the Kasteleyn-Fisher-Temperley theory of the dimer model is reminded in a fermionic field theory formulation and we show how this theory breaks down when monomers are introduced [79, 135]. This theory was used to compute the partition functions, as well as dimer and monomer correlation functions in a perturbative way, leading to exact correlation exponents in the thermodynamic limit [41, 43]. At the end of the section, the bosonic formulation of the dimer model is presented *via* the so-called height mapping. The model will be then interpreted as a Coulomb gas theory of electric and magnetic charges. This theory will be very useful in order to compare with exact results about dimer and monomer correlations performed in the section 4. Special attention will be paid to boundary conditions and corner effects in a CFT framework, which will be crucial in order to interpret finite size effects to the free energy.

2.1. Dimer model and nilpotent variables

A graph \mathcal{G} is a pair of sets (V, E) , where V is a finite set of vertices, and E is a finite set of non-oriented edges. We define the adjacent matrix (also called connectivity matrix) $A = (A_{ij})$, where the ij -entry is associated with the ordered pair of vertices (v_i, v_j) , then $A_{ij} = 1$ if v_i and v_j are joined by an edge, and 0 otherwise (*cf.* Fig. 1 for the square lattice). The perfect matching number is the number of configuration with the property that each site of the lattice is paired with exactly one of its linked neighbors [106]. In the language of theoretical physics, the enumeration of perfect matching of a planar graph \mathcal{G} is equivalent to compute the partition function of the dimer model on the given lattice. In the simplest form, the number of dimers is the same in all the configurations, and the partition function is given by the equally-weighted average over all possible dimer configurations ². In the following, we will include equal fugacities t for dimers, so that the

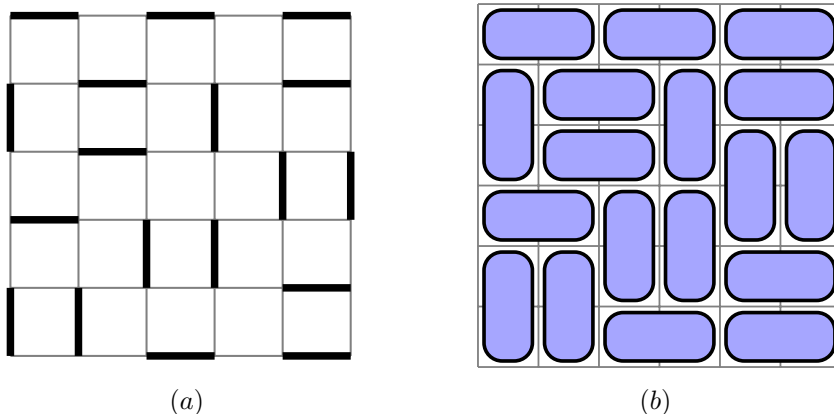


Figure 1: (a) Perfect matching of the square lattice, and (b) its "domino" representation. This combinatorial problem reduces to the calculation of the partition function Eq. (1) with $t = 1$.

average to be taken then includes weighting factors for dimers and we write the partition function as

$$Q_0[t] = \int \mathcal{D}[\eta] \exp(-\beta\mathcal{H}), \quad (1)$$

²Throughout this work, we will use the physics terminology and use the expression *perfect matching* in some specific cases.

where the Hamiltonian for the dimer written using commuting nilpotent variables (see Appendix A) can be written as a sum over every vertices (see Fig. 2), preventing two dimers to occupy the same site

$$\mathcal{H} = -\frac{t}{2} \sum_{ij} \eta_i A_{ij} \eta_j, \quad (2)$$

where A_{ij} is the adjacent matrix of the lattice considered. Let us put $\beta = 1$ in the following. The nilpotent variables can be seen as commuting Grassmann variables, or simply a product of two sets of standard Grassmann variables where $\eta_i = \theta_i \bar{\theta}_i$. The perfect matching number of the graph \mathcal{G} is equal to the partition function in the

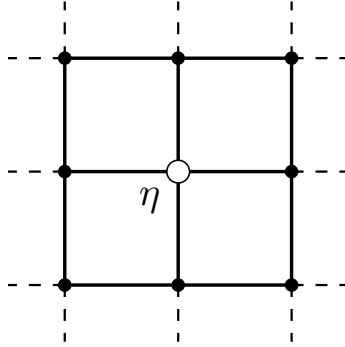


Figure 2: At every vertices, we put a nilpotent variable η , such that $\eta^2 = 0$ forbidden two dimers to occupy the same site.

case $t = 1$

$$\begin{aligned} Q_0[1] &= \int \mathcal{D}[\eta] \exp \left(\frac{1}{2} \sum_{ij} \eta_i A_{ij} \eta_j \right) = \int \mathcal{D}[\theta, \bar{\theta}] \exp \left(\frac{1}{2} \sum_{ij} \theta_i \bar{\theta}_i A_{ij} \theta_j \bar{\theta}_j \right) \\ &= \text{hf } A. \end{aligned} \quad (3)$$

We report the reader to the Appendix A for the definition of the haffnian of a matrix. In the second line we decomposed the nilpotent variables using two sets of Grassmann variables, and we finally found the well known graph theory result

$$\boxed{\text{perfect } \mathcal{G} = \text{hf } A.} \quad (4)$$

Considering holes in the perfect matching problem is equivalent to remove rows and columns at the positions of the holes in the adjacent matrix (see Fig. 3). The resulting combinatorial problem is called the near-perfect matching problem. The partition function of the dimer model with a fixed number of holes (monomers) can be written as

$$\begin{aligned} Q_n[1] &= \int \mathcal{D}[\theta, \bar{\theta}] \prod_{p=1}^n \theta_{q_p} \bar{\theta}_{q_p} \exp \left(\frac{1}{2} \sum_{ij} \theta_i \bar{\theta}_i A_{ij} \theta_j \bar{\theta}_j \right) \\ &= \int \mathcal{D}[\theta, \bar{\theta}] \exp \left(\frac{1}{2} \sum_{ij} \theta_i \bar{\theta}_i A_{ij}^{\setminus \{q_p\}} \theta_j \bar{\theta}_j \right) \\ &= \text{hf } A^{\setminus \{q_p\}}, \end{aligned} \quad (5)$$

where the index n stands for the number of monomers in $Q_n[t]$. Finally, the result is the same but now the matrix $A^{\setminus\{q_p\}}$ is the adjacent matrix of the original graph with positions of the n monomers removed. Suppose

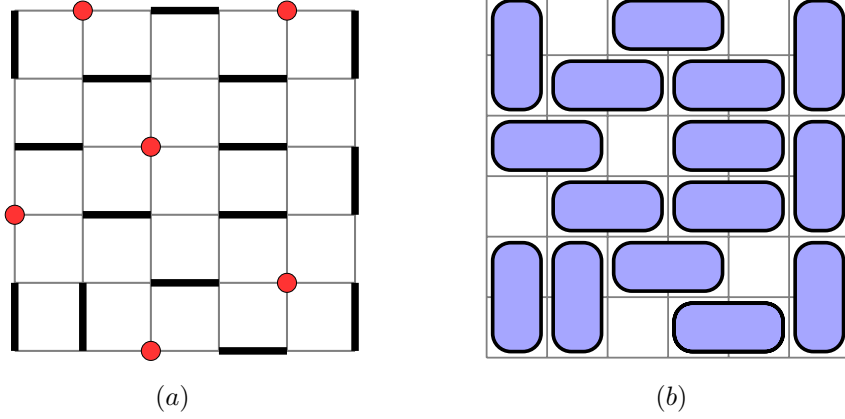


Figure 3: (a) Dimer model with 6 monomers, and (b) its "domino" representation.

we remove two sites q_1 and q_2 on the graph \mathcal{G} , then it is similar to introduce two nilpotent variables η_{q_1} and η_{q_2} on the lattice, the correlation function between these two monomers is then

$$\begin{aligned} \langle \eta_{q_1} \eta_{q_2} \rangle &= \langle (\theta_{q_1} \bar{\theta}_{q_1}) (\theta_{q_2} \bar{\theta}_{q_2}) \rangle = Q_0[1]^{-1} \int \mathcal{D}[\eta] \exp \left(\frac{1}{2} \sum_{ij} \theta_i \bar{\theta}_i A_{ij}^{\setminus(q_1, q_2)} \theta_j \bar{\theta}_j \right) \\ &= \text{hf} A^{\setminus(q_1, q_2)} \text{hf}^{-1} A, \end{aligned} \quad (6)$$

and more generally the n -point correlation function reads

$$\left\langle \prod_{p=1}^n \eta_{q_p} \right\rangle = \left\langle \prod_{p=1}^n \theta_{q_p} \bar{\theta}_{q_p} \right\rangle = \frac{\text{hf} A^{\setminus\{q_p\}}}{\text{hf} A}. \quad (7)$$

The partition function and correlations can be studied in the case $t \neq 1$ as well, in that case, the matrix elements of A are $a_{ij} = \pm t$ and the generalization is straightforward. Generally correlations between monomers are equal to correlations between nilpotent variables in this framework, which can be written in terms of a ratio between two haffnian. Unlike the determinant which can be computed by a $\mathcal{O}(L^3)$ time algorithm by Gauss elimination, there is no polynomial time algorithm for computing permanent. The problem of converting a permanent problem into a determinant problem is a long standing problem in pure mathematics, the simplest version of this problem, is called the Pólya permanent problem [121]. Given a $(0, 1)$ -matrix $A := (A_{ij})_{L \times L}$, can we find a matrix $B := (B_{ij})_{L \times L}$ such that $\text{perm} A = \det B$ (or equivalently $\text{hf} A = \text{pf} B$) where $B_{ij} = \pm A_{ij}$.

2.2. Haffnian to Pfaffian conversion and Kasteleyn solution

The close-packed dimer model can be solved on any planar lattice by using Pfaffian techniques. These techniques were introduced in the early sixties by Kasteleyn [79] and Temperley [135] and give a answer to the Pólya permanent problem for some particular conditions. The Kasteleyn theorem is a recipe to find a matrix³

³We will call this matrix the Kasteleyn matrix in the following.

K in such way that $\text{hf}A = \text{pf}K$, where the elements of the matrix are $K_{ij} = \pm 1$. Kasteleyn theorem is based on a special disposition of arrows on the edges of a planar graph⁴, the product of their orientation around any even-length closed path should be -1 . Such a disposition is given in Fig. 4(b) for the square lattice. We define an antisymmetric matrix K , where

$$K_{ij} = \begin{cases} 1 & \text{if the arrow points from } i \text{ to } j \\ -1 & \text{if the arrow points from } j \text{ to } i \\ 0 & \text{otherwise} \end{cases}$$

Kasteleyn theorem states that the perfect matching number of a given planar graph \mathcal{G} is given by

$$\text{perfect } \mathcal{G} = \text{hf}A = \text{pf}K, \quad (8)$$

which is equal to $\pm\sqrt{\det K}$. The \pm sign is chosen to make the perfect matching number positive, henceforth we will omit this sign in the rest of the article. Differently, this pfaffian can be express in terms of Grassmann variables (*cf.* Appendix A)

$$\text{pf}K = \int \mathcal{D}[a] \exp\left(\frac{1}{2} \sum_{i,j=1}^N a_i K_{ij} a_j\right). \quad (9)$$

For the square lattice, we can choose Boltzmann weights t_x and t_y for horizontal and vertical dimers, then the

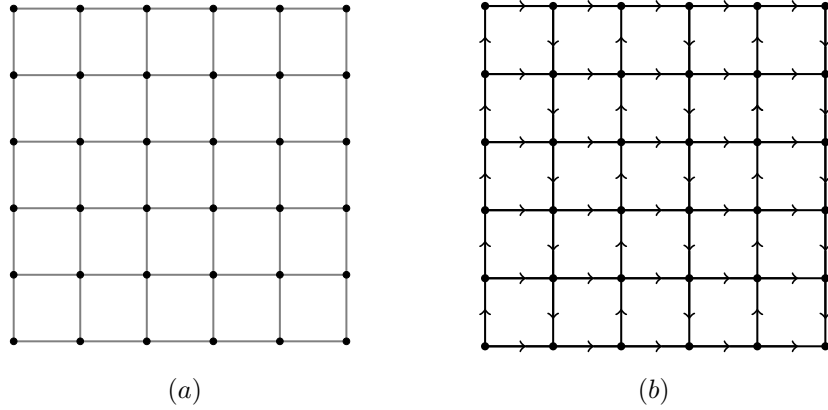


Figure 4: (a) Square lattice and (b) the orientation prescription of the Kasteleyn matrix.

pfaffian can be computed by using Fourier transform and Kasteleyn found for free boundary conditions (*cf.* [79] for details on calculations)

$$Q_0[t_x, t_y] = \prod_{p=1}^{M/2} \prod_{q=1}^{N/2} \left[4t_x^2 \cos^2 \frac{\pi p}{M+1} + 4t_y^2 \cos^2 \frac{\pi q}{N+1} \right]. \quad (10)$$

⁴This is a *condicio sine qua non* and the theorem is no longer valid for non-planar graph.

In table 1, we compute $Q_0[1, 1]$ using MATHEMATICA[®], for different M and N with $t_x = t_y = 1$ (perfect matching number). All these values can be numerically checked using diverse algorithms which enumerate all

$M \setminus N$	2	4	6	8	10	12
2	2	5	13	34	89	233
4	5	36	281	2245	18061	145601
6	13	281	6728	167089	4213133	106912793
8	34	2245	167089	12988816	1031151241	82741005829
10	89	18061	4213133	1031151241	258584046368	65743732590821
12	233	145601	106912793	82741005829	65743732590821	53060477521960000

Table 1: Perfect matching number $Q_0[1, 1]$ of the square lattice, for different M and N .

the possible configurations on the square lattice (see [101] for details). In the rest of the paper we will omit the labels t_x and t_y in the partition function and just keep Q_0 .

2.2.1. Entropy in the thermodynamic limit

The asymptotic form $L \rightarrow \infty$ of the partition function (for $M = N = L$) can be easily found from Eq. (10)

$$Q_0 \sim \exp \frac{GL^2}{\pi}, \quad (11)$$

where G is Catalan constant⁵. The factor G/π is the entropy by site of the dimer model on the square lattice. This entropy can also be calculated for other bipartite lattice like the honeycomb lattice, and for non-bipartite lattice like triangular, Kagomé lattice and triangular Kagomé lattice. The pfaffian method can be used to compute the partition function of the dimer model on various geometries and boundary conditions leading to different values of the entropy (*cf.* [143] for review), as long as the lattice has a Kasteleyn orientation (*i.e.* planar according to the Kasteleyn theorem) and as long as $N \times M$ is even. Obviously it is impossible to fill an odd size lattice with dimers, without leaving one site empty. We shall take notice later that the form of the free energy is strongly dependent of the parity of the lattice.

2.2.2. Probabilities and correlations

The Kasteleyn matrix is a very powerful objet, which gives us all the details about probabilities of presence of dimers [43]. For example the occupation probability $\mathbb{P}[i \rightarrow j]$ of a dimer on the link ij is

$$\mathbb{P}[i \rightarrow j] = K_{ij} \times K_{ij}^{-1}, \quad (12)$$

where K_{ij} and K_{ij}^{-1} are the corresponding matrix elements of the Kasteleyn matrix and its inverse. The probability of two dimers on the links ij and mn is

$$\mathbb{P}[i \rightarrow j | m \rightarrow n] = \det \begin{pmatrix} K_{ij}^{-1} & K_{im}^{-1} \\ K_{mj}^{-1} & K_{mn}^{-1} \end{pmatrix}. \quad (13)$$

In the rest of the paper, we shall use the term *correlation* even though this quantity is a normalized probability. Correlations between more than two dimers are available using the Kasteleyn matrix as well. It can be shown

⁵ $G = 1^{-2} - 3^{-2} + 5^{-2} - 7^{-2} + \dots = 0.915965594\dots$

[41, 43] that dimer-dimer correlations on the square lattice decrease as the inverse square of the distance between the two dimers in the thermodynamic limit

$$\mathbb{P}(r) \sim r^{-2}. \quad (14)$$

Furthermore it has been also shown that correlations are always critical [80] for bipartite lattices and *a contrario* exponential for non-bipartite lattices as the triangular lattice for example, where the fermionic theory underlying is a massive theory [39].

2.3. Monomer correlation functions

Throughout this work the monomer-monomer correlation function C will be defined as the ratio of the number of configurations with monomers at fixed positions to the number of configurations without monomers. Thus computing a monomer-monomer correlation is *stricto sensu* equivalent to compute the partition function with two sites (and all the links connected to these sites) deleted. Since such a graph is still planar, Kasteleyn's construction is still applicable. The one complication is that we must ensure that on the new lattice with deleted sites, the number of arrows is still clockwise-odd. If all the monomers are located on the boundary of the lattice at ordinate $\{x_i\}$, there is no non-local defect lines between monomers (see Fig. 5), and the modified matrix $K^{\setminus\{x_i\}}$ defined from K by removing all the rows and columns corresponding to the monomers positions has still the proper Kasteleyn orientation. Then the pfaffian of this modified Kasteleyn matrix $K^{\setminus\{x_i\}}$ gives us the partition function of the dimer model with fixed monomer positions. It follows that the correlation function between two monomers on the boundary is

$$C(x_1, x_2) := \frac{Q_2(x_1, x_2)}{Q_0} = \text{pf}(K^{-1}K^{\setminus(x_1, x_2)}) = \langle a_i a_j \rangle, \quad (15)$$

where x_1 and x_2 are the positions of the two monomers. This pfaffian has been computed by Priezzhev and Ruelle (*cf.* [123] for details) in the thermodynamic limit for a arbitrary number of monomers at positions $\{x_i\}$, using a perturbative analysis of the matrix $K^{\setminus\{x_i\}}$ around the original Kasteleyn matrix K . The result for the $2n$ -point correlation is given by

$$C(x_1, x_2 \dots x_{2n}) = \text{pf } C, \quad (16)$$

where the matrix element $C_{ij} := C(x_i, x_j)$ is the 2-point function of a $1d$ complex free-fermion, equal to

$$C_{ij} = -\frac{2}{\pi|x_i - x_j|}, \quad (17)$$

if x_i and x_j are on opposite sublattices and $C_{ij} = 0$ otherwise. For monomers in the bulk, the things are much more complicated. One sees that the product of arrows around a deleted site is now equal to $+1$ (see Fig. 5). We thus must construct a string of reversed arrows from one monomer to the second (see Fig. 5(b)). As long as the arrows are chosen to make all plaquette clockwise odd, the correlation is independent of the choice of the path. In the general case of bulk monomers, the relation Eq. (15) is no longer correct, because the matrix $K^{\setminus(x_i, x_j)}$ is no more a Kasteleyn matrix. Then correlations between two monomers defined by $Q_2(x_i, x_j)/Q_0$ is not equal to correlations between two Grassmann variables $\langle a_i a_j \rangle$, but disorder operators must be add

$$\frac{Q_2(x_i, x_j)}{Q_0} = \left\langle a_i \exp \left(2 \sum_{pq} K_{pq} a_p a_q \right) a_j \right\rangle, \quad (18)$$

where the sum is over all the links connecting sites i and j , to take account of the reversing line between the two monomers. Using a pfaffian perturbative analysis it was shown that monomer correlations decreases at the

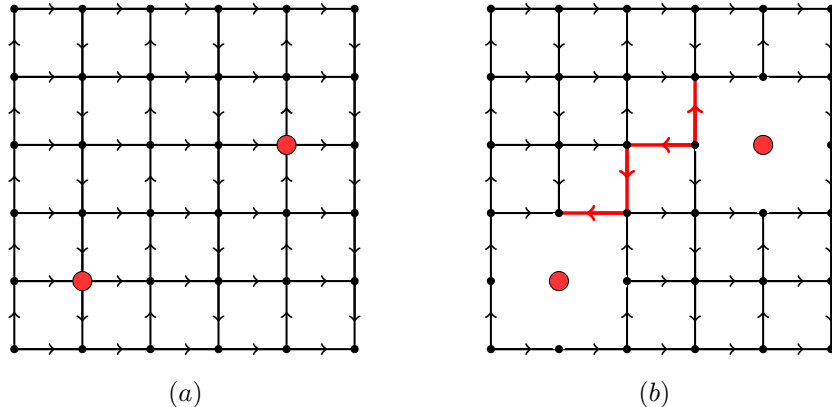


Figure 5: Modification of the Kasteleyn matrix in the presence of two monomers. The monomers (red dots) destroy the corresponding links and the orientation (a) has to be changed to respect the proper orientation (b).

thermodynamic limit as [41, 43]

$$C(r) \sim r^{-1/2}. \quad (19)$$

This result is very similar to the construction of the spin correlation functions in the Ising model in terms of fermionic variables [78, 122]. In fact, on the square lattice, the monomer-monomer correlations was shown to have the same long-distance behavior as the spin-spin correlations in two decoupled Ising models, explained by the deep relation between the two correlation functions for the square lattice given by Perk and Au-Yang [6]. These disorder operators are absent in the haffnian theory Eq. (7), and are the price to pay to solve the problem analytically.

2.4. Mapping to a bosonic theory

2.4.1. Height mapping and Coulomb gas formalism

To any dimer covering we can associate a height on the dual lattice (on the plaquette) which is defined as follows [149, 103, 65, 62]. When encircling an even vertex in the positive (counterclockwise) direction, the height h increases by $+1$ upon crossing an empty edge and decreases by -3 upon crossing an edge that is covered by a dimer (*cf.* Fig. 6). It is easy to notice that for the allowed configuration the average values h_{vertex} that the height variables can take at a given site of the direct lattice (a vertex) are $h_{\text{vertex}} = \pm 3/2$ or $h_{\text{vertex}} = \pm 1/2$.⁶ On the other hand, a uniform shift of all the heights by one unit leads to an equivalent state. This mapping works *stricto sensu* for the close packed case. We will find it simpler to work with the rescaled height field $\phi = \frac{\pi}{2}h$. By fixing the rescaled height at an arbitrary point, *e.g.* $\phi(0) = 0$, these rules define the entire height function $\phi(\vec{r})$ uniquely. By integrating out the short distance fluctuations, one obtains an effective quadratic action \mathcal{S} for the bulk height field $\phi(\vec{r})$, defined in the continuum, which corresponds to the long-wavelength modes

$$\boxed{\mathcal{S}[\phi] = \frac{g}{2} \int dx dy (\nabla \phi)^2.} \quad (20)$$

⁶We mention here that the height mapping remains valid for the interacting dimer model [4, 3, 115, 33], and it can be showed that, at the Kosterlitz-Thouless point, the interactions renormalize the free theory to another value of the stiffness $g = 2/\pi$.

-2	-1	-2	-1	-2
-3	-4	-3	0	1
-2	-1	-2	-1	2
1	0	-3	0	1
2	-1	-2	-1	-2

Figure 6: Height mapping of the dimer model with free boundary conditions. For pedagogical purposes we will keep the field h on the figures.

Here g a constant which controls the stiffness of the height model. It is *a priori* unknown. The field has to be invariant under the transformation $\phi = \phi + 2\pi n$ to respect lattice symmetries. The derivation of this gaussian field has been actually done rigorously by mathematicians [85, 86]. Electric charges e correspond to vertex operators appearing in the Fourier expansion of any operator periodic in the height field. Dual magnetic charges m correspond to a dislocation in the height field and correspond to the dual vertex operator

$$\begin{aligned} V_e(z) &= : e^{ie\phi} : \\ V_m(z) &= : e^{im\psi} : \end{aligned} \quad (21)$$

where ψ is the dual field of ϕ and defined as

$$\partial_i \psi = \epsilon_{ij} \partial_j \phi. \quad (22)$$

These operators are primary operators of the $c = 1$ CFT. The scaling dimension associated to the insertion of a particle with electromagnetic charge (e, m) is given by

$$x_g(e, m) = \frac{e^2}{4\pi g} + \pi g m^2. \quad (23)$$

For example, two monomers on opposite sublattices correspond to two charges $m = 1$ and $m = -1$. It is known from exact results [41, 43] that, the exponent for bulk monomer-monomer correlations is $1/2$, it fixes $g_{\text{free}} = 1/4\pi$ for the stiffness constant of the gaussian field theory describing the free dimer model. We saw previously that bulk dimer-dimer exponent is 2. Hence the bulk monomer and dimer scaling dimensions defined by $x_b^{(m)} := x_{\frac{1}{4\pi}}(0, 1)$ and $x_b^{(d)} := x_{\frac{1}{4\pi}}(1, 0)$ are

$$\text{free dimer : } g_{\text{free}} = \frac{1}{4\pi} \rightarrow \begin{cases} x_b^{(d)} := x_{\frac{1}{4\pi}}(1, 0) = 1 \\ x_b^{(m)} := x_{\frac{1}{4\pi}}(0, 1) = 1/4. \end{cases} \quad (24)$$

In this theory the conformal spin of an operator is defined by $s(e, m) = em$, then monomers and dimers are spinless particles but fermions which are order-disorder composite operators [78] have magnetic and electric charges and carry spins $1/2$. The fermion operator has then scaling dimension $x_{\frac{1}{4\pi}}(1/2, 1) = 1/2$. It is also possible to define parafermion operators which obey fractional statistics [51] for particular values of the stiffness

g. The use of such a mapping to study correlation functions dates back to Blöte, Hilhorst, and Nienhuis [112, 16]. The neutral 2-point correlation functions for vertex operators are then given by the standard formula [111]

$$\begin{aligned}\langle V_{m=+1}(z)V_{m=-1}(0) \rangle &\sim z^{-2x_{\frac{1}{4\pi}}(0,1)} = z^{-1/2} \\ \langle V_{e=+1}(z)V_{e=-1}(0) \rangle &\sim z^{-2x_{\frac{1}{4\pi}}(1,0)} = z^{-2}.\end{aligned}\quad (25)$$

The general monomer $2n$ -point function is given by the product

$$\langle V_{m_1=\pm 1}(z_1)\dots V_{m_{2n}=\pm 1}(z_{2n}) \rangle \sim \frac{\prod_{i<j}(b_i - b_j)^{1/2} \prod_{k<l}(w_k - w_l)^{1/2}}{\prod_{p<q}(b_p - w_q)^{1/2}}, \quad (26)$$

where $\{b_k\}$ and $\{w_k\}$ are the sets of the even/odd sublattice coordinates. In this Coulomb gas interpretation of the dimer model, monomers located on the same sublattice are seen as repelling equal charges, and monomers on opposite sublattice are seen as attractive opposite charges. It is known from exact results [123, 5] that, the exponent for monomer correlations is 1 in the case (see Eq. (16)) where the monomers are restricted to live on a boundary. Hence the surface monomer scaling dimension is $x_s^{(m)} := 1/2$.

2.4.2. Rectangular geometry and boundary conditions

On Fig. 7, we show a configuration of dimers on the square lattice with free boundary conditions. The choice of these conditions impose very specific boundary conditions for the height variable. Indeed, we observe that the value of the height h is $(..101..)$ along the boundary until the corner and $(..-10-1..)$ along the next boundary [130] (a similar analysis has been done for the strip geometry [132, 133]). Then we have, from the

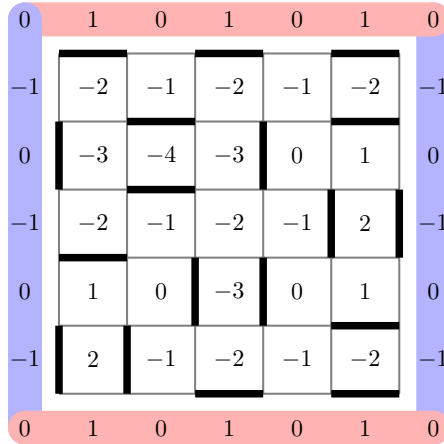


Figure 7: Height mapping of the dimer model with free boundary conditions. The different values of the height h on each sides of each corner are induced by a *bcc* operator of scaling dimension $1/32$. The dimension does not change if one chooses a rectangle $M \neq N$.

point a view of the field theory two different averaged boundary conditions either sides of the corner, let us call the boundary fields $h_b = 1/2$ and $\bar{h}_b = -1/2$. The proper way to understand how corners change the behavior of the height field is through boundary CFT (*cf.* [61] for introduction). Hence it is natural to introduce local operators [23] acting on the corners of the domain, these objects called *boundary condition changing* operators (*bcc*) can be showed to be primary operators of the CFT [24]. A careful analysis shows that the difference

of boundary conditions has non negligible consequences in the thermodynamic limit and the precise procedure based on the contribution of these operators on the free energy can be found in [132]. It has been shown that the dimension of the bcc operator which creates a field shift of value $\Delta\phi_b = \frac{\pi}{2}(h_b - \bar{h}_b) = \phi_b - \bar{\phi}_b$ on the corner is

$$h_{bcc} = \frac{g}{2\pi} \Delta\phi_b^2, \quad (27)$$

with $g_{\text{free}} = 1/4\pi$ here. In the previous situation without any monomer, the corner shift in the height h is equal to $\Delta h_b = 1$ then $\Delta\phi_b = \pi/2$, hence the dimension of the corner bcc operator is $h_{bcc} = 1/32$. Furthermore, the addition of a monomer on the boundary or at the corner will change the value of the field, and we will behold further that it will be relevant in order to study quantities as the free energy and correlation functions. A general framework to study partition functions and conformal boundary states on the rectangular geometry with different boundary conditions in a boundary CFT framework has been developed recently [17, 18]. In the section 4, finite size effects to the free energy for the free and interacting cases will be study in this CFT framework, and the influence of these bcc operators will be crucial to identify the correct underlying central charge of the theory. Furthermore the presence of monomers on the boundaries or at the corners will change again the values of the bcc operators which will be important for the study of surface and corner correlation functions.

3. Exact partition function and corner free energy

In this section, the fully-detailed Grassmann solution of the dimer model with an arbitrary number of monomers is presented, which will lead to the exact form of correlation functions in a pfaffian formulation. In particular, we show that the problem become simpler when we consider boundary monomers, and a closed expression for correlations can be found. Hereinafter the solution of the dimer model on a odd size lattice with one boundary monomer is introduced, in agreement with the Tzeng-Wu solution [136]. Those solutions will be used to extract finite-size scaling behaviors of the free energy in a CFT framework, where *boundary changing conditions* operators has to be carefully study to infer the central charge of the model, in contradiction with a recent article [69].

3.1. Plechko pfaffian solution

Here we just recall the framework of the Plechko solution [56, 57] of the dimer model. As we have seen in the section 2, the partition function can be written for a general graph using nilpotent variables

$$Q_0 = \int \mathcal{D}[\eta] \exp \left(\frac{1}{2} \sum_{i,j=1}^N \eta_i A_{ij} \eta_j \right). \quad (28)$$

We are now working on the square lattice with free boundary conditions, then the partition function reads

$$Q_0 = \int \mathcal{D}[\eta] \prod_{m,n}^L (1 + t_x \eta_{mn} \eta_{m+1n}) (1 + t_y \eta_{mn} \eta_{mn+1}), \quad (29)$$

where t_x and t_y are the horizontal and vertical Boltzmann weight, and m and n refer to the coordinates. The partition function can be written using Grassmann variables (see Appendix B for details), this leads to a block representation of the action in the momentum space, for momenta inside the reduced sector $1 \leq p, q \leq L/2$.

The four components of these vectors will be written c_α^μ with $\mu = 1 \cdots 4$, leading to

$$Q_0 = \int \mathcal{D}[c] \exp S_0[c], \quad (30)$$

with $S_0[c] = \frac{i}{2} c_\alpha^\mu M_\alpha^{\mu\nu} c_\alpha^\nu$ ⁷, where the antisymmetric matrix M is defined by

$$M_\alpha = \begin{pmatrix} 0 & 0 & a_y(q) & a_x(p) \\ 0 & 0 & -a_x(p) & a_y(q) \\ -a_y(q) & a_x(p) & 0 & 0 \\ -a_x(p) & -a_y(q) & 0 & 0 \end{pmatrix} \quad (31)$$

with

$$\begin{aligned} a_x(p) &= 2t_x \cos \frac{\pi p}{L+1}, \\ a_y(q) &= 2t_y \cos \frac{\pi q}{L+1}. \end{aligned} \quad (32)$$

This matrix can be written as

$$M_\alpha = a_x(p)\Gamma_x + a_y(q)\Gamma_y, \quad (33)$$

where the matrices Γ_x and Γ_y are

$$\Gamma_x = \begin{pmatrix} 0 & 0 & 0 & 1 \\ 0 & 0 & -1 & 0 \\ 0 & 1 & 0 & 0 \\ -1 & 0 & 0 & 0 \end{pmatrix}, \quad \Gamma_y = \begin{pmatrix} 0 & 0 & 1 & 0 \\ 0 & 0 & 0 & 1 \\ -1 & 0 & 0 & 0 \\ 0 & -1 & 0 & 0 \end{pmatrix}, \quad (34)$$

with $\Gamma_x^2 = \Gamma_y^2 = -1$. Hence the expression Eq. (119) is directly related to the pfaffian of the matrix M (*cf.* A for details) and is simply equal to

$$\begin{aligned} Q_0 &= \prod_{\alpha} \text{pf} M_\alpha \\ &= \prod_{p,q}^{L/2} [a_x(p)^2 + a_y(q)^2]. \end{aligned} \quad (35)$$

Finally one simply obtains the following well known result

$$Q_0 = \prod_{p,q=1}^{L/2} \left[4t_x^2 \cos^2 \frac{\pi p}{L+1} + 4t_y^2 \cos^2 \frac{\pi q}{L+1} \right]. \quad (36)$$

The fermionization can also be performed for toroidal boundary conditions. We refer here to the experience with the $2d$ Ising model on a torus [118]. The final result can be written in terms of a combination of the periodic-antiperiodic boundary conditions for fermions $c_{M+1n=\pm c_{1n}}$ and $c_{mN+1=\pm c_{m1}}$.

⁷Repeated indices are implicitly summed over.

3.2. Pfaffian solution with $2n$ monomers.

3.2.1. General case

Let us now consider the case where an even⁸ number of monomers are present on the lattice at different positions $\mathbf{r}_i = (m_i, n_i)$ with $i = 1, \dots, 2n$. The partition function $Q_{2n}(\{\mathbf{r}_i\})$ is the number of all possible configurations with the constraint imposed by the fixed monomers. This quantity can be evaluated by inserting nilpotent variables $\eta_{m_i n_i}$ in the partition function, which prevents possible dimers to occupy sites \mathbf{r}_i . It can be useful to introduce an additional Grassmann variable h_i such that $\eta_{m_i n_i} = \int dh_i \exp(h_i \eta_{m_i n_i})$. These insertions are performed at point \mathbf{r}_i in Q_0 , and the integration over $\eta_{m_i n_i}$ modifies $L_{m_i n_i} \rightarrow L_{m_i n_i} + h_i$. However, by moving the dh_i variable to the left of the remaining ordered product, a minus sign is introduced in front of each \bar{b}_{mn_i-1} in \bar{B}_{mn_i} for all $m > m_i$. We can replace \bar{b}_{mn_i-1} by $\epsilon_{mn_i} \bar{b}_{mn_i-1}$ such that $\epsilon_{mn_i} = -1$ for $m > m_i$, and $\epsilon_{mn_i} = 1$ otherwise. The integration is then performed on the remaining variables (a, \bar{a}, b, \bar{b}) as usual, so that $Q_{2n}(\{\mathbf{r}_i\})$ can be expressed as a Gaussian form, with a sum of terms corresponding to the monomer insertion, resulting to the following form for the the partition function

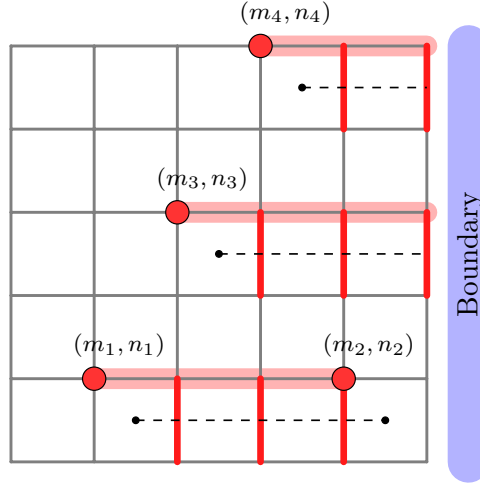


Figure 8: Typical dimer configuration for a 6×6 square lattice. The dashed line is the extra term that arises from moving towards the border the Grassmann field conjugated to the monomer. This is equivalent to change the sign of the t_y couplings (red links) from the monomers to the boundary. When two monomers are located on the same horizontal line, the change of sign concerns only the couplings between the two monomers.

$$Q_{2n}(\{\mathbf{r}_i\}) = \int \mathcal{D}[c] \mathcal{D}[h] \exp \left[S_0 + \sum_{\mathbf{r}_i} c_{m_i n_i} h_i + 2t_y \sum_{\mathbf{r}_i, m=m_i+1}^L (-1)^{m+1} c_{mn_i-1} c_{mn_i} \right]. \quad (37)$$

where $\int \mathcal{D}[c] \mathcal{D}[c] = \int \prod_{mn} dc_{mn} \prod_i dh_i$ where the index i runs over the set of positions $\mathbf{r}_i = (m_i, n_i)$ of the $2n$ monomers. The inclusion or monomers is equivalent to inserting a magnetic field h_i at points \mathbf{r}_i , as well as a sum of quadratic terms $c_{mn_i-1} c_{mn_i}$ running from the hole position to the boundary on the right (see Fig. 8). Another possibility would be to join two monomers by a line of terms by moving $dh_{m_i n_i}$ until $dh_{m_j n_j}$ as in the Kasteleyn theory. In this case, the additional quadratic terms in the action starting from \mathbf{r}_i and ending on the

⁸The case with an odd number of monomers can be studied as well as we shall see later.

boundary have to be treated in the computation of the Grassmannian integral. We first rewrite S_0 in the Fourier space using the block partition label $\alpha = (p, q)$ for momenta p and q inside the reduced sector $1 \cdots L/2$, and vectors $\mathbf{c}_\alpha =^t (c_{pq}, c_{-pq}, c_{p-q}, c_{-p-q})$. Also the 4 components of vector \mathbf{c}_α will be written c_α^μ where $\mu = 1 \cdots 4$. Then $S_0 = \frac{i}{2} c_\alpha^\mu M_\alpha^{\mu\nu} c_\alpha^\nu$, where the antisymmetric quadratic form M_α is defined by Eq. (31). The part of the field interaction can be Fourier transform as before with a linear field H_{pq} depending on h_i s and we obtain

$$\sum_{\mathbf{r}_i} c_{m_i, n_i} h_i = \sum_{p, q=1}^L c_{pq} H_{pq} = \sum_{\alpha, \mu} c_\alpha^\mu H_\alpha^\mu. \quad (38)$$

The last contribution connecting the monomers to the boundary can be written as $\frac{i}{2} c_\alpha^\mu V_{\alpha\beta}^{\mu\nu} c_\beta^\nu$, with matrix $V_{\alpha\beta} = V_{pq, p'q'}$ given by

$$V_{pq, p'q'} = \sum_{\mathbf{r}_i} \frac{8t_y(-1)^{n_i}}{(L+1)^2} \left\{ \sum_{m=m_i+1}^L \sin \frac{\pi p m}{L+1} \sin \frac{\pi p' m}{L+1} \right\} \left[\sin \frac{\pi q(n_i-1)}{L+1} \sin \frac{\pi q' n_i}{L+1} - \sin \frac{\pi q'(n_i-1)}{L+1} \sin \frac{\pi q n_i}{L+1} \right].$$

The different components $V_{\alpha\beta}^{\mu\nu}$ are given implicitly, for the first elements, by $V_{\alpha\beta}^{11} = V_{pq, p'q'}$, $V_{\alpha\beta}^{12} = V_{pq, -p'q'}$, $V_{\alpha\beta}^{21} = V_{-pq, p'q'}$, and so on. Then the total fermionic action contains three terms

$$S = \frac{i}{2} c_\alpha^\mu M_\alpha^{\mu\nu} c_\alpha^\nu + \frac{i}{2} c_\alpha^\mu V_{\alpha\beta}^{\mu\nu} c_\beta^\nu + c_\alpha^\mu H_\alpha^\mu. \quad (39)$$

The first two terms contain only modes of the same sector α , and the last connects modes from different sectors α and β . Matrices $M_\alpha^{\mu\nu}$ and $V_{\alpha\beta}^{\mu\nu}$ are antisymmetric: $M_\alpha^{\mu\nu} = -M_\alpha^{\nu\mu}$ and $V_{\alpha\beta}^{\mu\nu} = -V_{\beta\alpha}^{\nu\mu}$. Also $V_{\alpha\alpha} = 0$. Then the quantity $Q_{2n}(\{\mathbf{r}_i\})$ can be formally written as

$$\begin{aligned} Q_{2n}(\{\mathbf{r}_i\}) &= \int \mathcal{D}[c] \mathcal{D}[h] \exp \left(\frac{i}{2} c_\alpha^\mu [M_\alpha^{\mu\nu} \delta_{\alpha\beta} + V_{\alpha\beta}^{\mu\nu}] c_\beta^\nu + c_\alpha^\mu H_\alpha^\mu \right) \\ &= \int \mathcal{D}[c] \mathcal{D}[h] \exp \left(\frac{i}{2} c_\alpha^\mu W_{\alpha\beta}^{\mu\nu} c_\beta^\nu + c_\alpha^\mu H_\alpha^\mu \right), \end{aligned} \quad (40)$$

with $W_{\alpha\beta}^{\mu\nu} = \delta_{\alpha\beta} M_\alpha^{\mu\nu} + V_{\alpha\beta}^{\mu\nu}$ (cf. Fig. 9(a)). By construction, W is antisymmetric and satisfies $W_{\alpha\beta}^{\mu\nu} = -W_{\beta\alpha}^{\nu\mu}$. This matrix can be represented as a block matrix of global size $L^2 \times L^2$

$$W = \underbrace{\begin{pmatrix} \underbrace{M_{\alpha=(1,1)}}_{4 \times 4 \text{ matrix}} & V_{(1,1),(1,2)} & V_{(1,1),(1,3)} & \cdots \\ -V_{(1,1),(1,2)} & V_{(1,2)} & V_{(1,2),(1,3)} & \cdots \\ -V_{(1,1),(1,3)} & -V_{(1,2),(1,3)} & M_{(1,3)} & \cdots \\ \vdots & & & \ddots \end{pmatrix}}_{L^2/4 \text{ blocks}} \quad (41)$$

where each of the $(L^2/4) \times (L^2/4)$ blocks is a 4×4 matrix. Labels α are ordered with increasing momentum $(1, 1), (1, 2) \cdots (1, L/2), (2, 1) \cdots$. In the action the linear terms in c_α^μ can be removed using a linear change of variables $c_\alpha^\mu \rightarrow c_\alpha^\mu + g_\alpha^\mu$, where g_α^μ are Grassmann constants. After some algebra, we find the correct values for the constants that eliminate the linear contribution are given by $g_\alpha^\mu = i(W^{-1})_{\alpha\beta}^{\mu\nu} H_\beta^\nu$. After substitution of these values in the overall integral, and a rescaling of variables $c_\alpha \rightarrow c_\alpha/\sqrt{i}$, the action becomes a product over

variables c and h_i

$$\begin{aligned} Q_{2n}(\{\mathbf{r}_i\}) &= \int \mathcal{D}[c] \mathcal{D}[h] \exp \left[\frac{1}{2} c_\alpha^\mu W_{\alpha\beta}^{\mu\nu} c_\beta^\nu - \frac{i}{2} (W^{-1})_{\alpha\beta}^{\mu\nu} H_\alpha^\mu H_\beta^\nu \right] \\ &= \text{pf}(W) \int \mathcal{D}[h] \exp \left[-\frac{i}{2} (W^{-1})_{\alpha\beta}^{\mu\nu} H_\alpha^\mu H_\beta^\nu \right]. \end{aligned}$$

The fields H_α^μ can be expressed with h_i as $H_\alpha^\mu = \sum_{i=1}^{2n} \Lambda_{i,\alpha}^\mu h_i$, where coefficients $\Lambda_{i,\alpha}^\mu$ can be rewritten using a 4-dimensional vector, such as

$$\Lambda_{\mathbf{i},\alpha} = \frac{2}{L+1} \sin \frac{\pi p m_i}{L+1} \sin \frac{\pi q n_i}{L+1} \Lambda_{\mathbf{i}} =: r_i(\alpha) \Lambda_{\mathbf{i}}, \quad (42)$$

where the vector

$$\Lambda_{\mathbf{i}} = \begin{pmatrix} i^{m_i+n_i} \\ -i^{-m_i+n_i} \\ -i^{m_i-n_i} \\ i^{-m_i-n_i} \end{pmatrix}, \quad (43)$$

depends only on the location parity of the monomer \mathbf{r}_i in the bulk. Functions $r_i(\alpha)$ are normalized $\sum_\alpha r_i(\alpha) r_j(\alpha) = \delta_{ij}$. Then we obtain the following formal and compact expression for $Q_{2n}(\{\mathbf{r}_i\})$

$$\begin{aligned} Q_{2n}(\{\mathbf{r}_i\}) &= \text{pf}(W) \int \mathcal{D}[h] \exp \left(\frac{1}{2} \sum_{i,j} h_i h_j \Lambda_{i,\alpha}^\mu (W^{-1})_{\alpha\beta}^{\mu\nu} \Lambda_{j,\beta}^\nu \right) \\ &=: \text{pf}(W) \int \mathcal{D}[h] \exp \left(\frac{1}{2} \sum_{i,j} h_i h_j C_{ij} \right). \end{aligned} \quad (44)$$

Finally, we found a pfaffian expression of the partition function

$$\boxed{Q_{2n}(\{\mathbf{r}_i\}) = \text{pf}(W) \text{pf}(C)}. \quad (45)$$

We verify easily that the matrix C is antisymmetric by using the antisymmetry property of W or W^{-1}

$$\begin{aligned} C_{ji} &= \Lambda_{j,\alpha}^\mu (W^{-1})_{\alpha\beta}^{\mu\nu} \Lambda_{i,\beta}^\nu = \Lambda_{j,\beta}^\nu (W^{-1})_{\beta\alpha}^{\nu\mu} \Lambda_{i,\alpha}^\mu \\ &= -\Lambda_{j,\beta}^\nu (W^{-1})_{\alpha\beta}^{\mu\nu} \Lambda_{i,\alpha}^\mu \\ &= -C_{ij}. \end{aligned} \quad (46)$$

Then, C_{ij} can be formally expressed as a scalar product $C_{ij} = \sum_{\alpha,\beta} \langle \Lambda_{\mathbf{i},\alpha} | W_{\alpha,\beta}^{-1} | \Lambda_{\mathbf{j},\beta} \rangle$. Q_{2n} is therefore a product of two pfaffians where the monomer locations are specified in matrix W . The matrix V can be rewritten using additional matrices after considering the different components (μ, ν) . We can indeed express V using four functions $u_k^{a,s}(\alpha, \beta)$, and $v_k^{a,s}(\alpha, \beta)$, for each monomer at location $\mathbf{r}_k = (m_k, n_k)$, with $m_k < L$, and such that

$$V_{\alpha\beta} = -2t_y \sum_{\mathbf{r}_k} \sum_{c,c'} u_k^c(\alpha, \beta) \Gamma_{cc'} v_k^{c'}(\alpha, \beta), \quad (47)$$

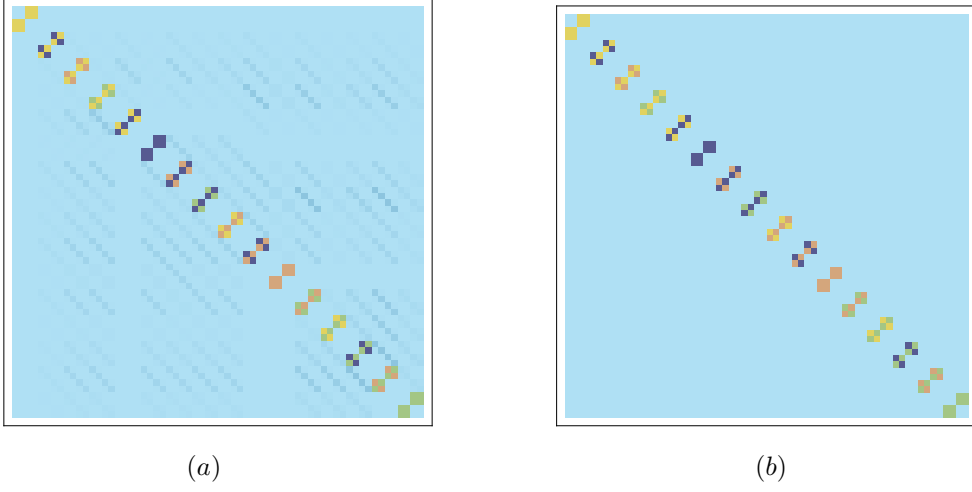


Figure 9: (a) Graphical representation of the matrix $W = M + V$. (b) When the monomers are on the boundaries of the domain, the off diagonal term V vanishes and the matrix W reduces to the matrix M .

where the $\Gamma_{cc'}$ are defined as

$$\Gamma_{sa} = \begin{pmatrix} 1 & 0 & 0 & 0 \\ 0 & 1 & 0 & 0 \\ 0 & 0 & -1 & 0 \\ 0 & 0 & 0 & -1 \end{pmatrix}, \Gamma_{aa} = \begin{pmatrix} 0 & 1 & 0 & 0 \\ 1 & 0 & 0 & 0 \\ 0 & 0 & 0 & -1 \\ 0 & 0 & -1 & 0 \end{pmatrix}, \Gamma_{ss} = \begin{pmatrix} 0 & 0 & 1 & 0 \\ 0 & 0 & 0 & 1 \\ -1 & 0 & 0 & 0 \\ 0 & -1 & 0 & 0 \end{pmatrix}, \Gamma_{as} = \begin{pmatrix} 0 & 0 & 0 & 1 \\ 0 & 0 & 1 & 0 \\ 0 & -1 & 0 & 0 \\ -1 & 0 & 0 & 0 \end{pmatrix}.$$

Functions u and v are given by

$$\begin{aligned} u_k^s(\alpha, \beta) &= \frac{2}{L+1} \sum_{m=m_k+1}^L \sin \frac{\pi p m}{L+1} \sin \frac{\pi p' m}{L+1}, \\ u_k^a(\alpha, \beta) &= \frac{2}{L+1} \sum_{m=m_k+1}^L (-1)^{m+1} \sin \frac{\pi p m}{L+1} \sin \frac{\pi p' m}{L+1}, \\ v_k^s(\alpha, \beta) &= \frac{2}{L+1} \left[\sin \frac{\pi q n_k}{L+1} \sin \frac{\pi q' (n_k - 1)}{L+1} + \sin \frac{\pi q' n_k}{L+1} \sin \frac{\pi q (n_k - 1)}{L+1} \right], \\ v_k^a(\alpha, \beta) &= \frac{2(-1)^{n_k}}{L+1} \left[\sin \frac{\pi q n_k}{L+1} \sin \frac{\pi q' (n_k - 1)}{L+1} - \sin \frac{\pi q' n_k}{L+1} \sin \frac{\pi q (n_k - 1)}{L+1} \right]. \end{aligned} \quad (48)$$

More explicitly the result is

$$\begin{aligned}
u_k^s(\alpha, \beta) &= \frac{\sin \frac{\pi(p-p')(L+1/2)}{L+1} - \sin \frac{\pi(p-p')(m_k+1/2)}{L+1}}{2(L+1) \sin \frac{\pi(p-p')}{2(L+1)}} - \frac{\sin \frac{\pi(p+p')(L+1/2)}{L+1} - \sin \frac{\pi(p+p')(m_k+1/2)}{L+1}}{2(L+1) \sin \frac{\pi(p+p')}{2(L+1)}}, \\
u_k^a(\alpha, \beta) &= - \frac{\cos \frac{\pi(p-p')(L+1/2)}{L+1} - (-1)^{m_k} \cos \frac{\pi(p-p')(m_k+1/2)}{L+1}}{2(L+1) \cos \frac{\pi(p-p')}{2(L+1)}} + \frac{\cos \frac{\pi(p+p')(L+1/2)}{L+1} - (-1)^{m_k} \cos \frac{\pi(p+p')(m_k+1/2)}{L+1}}{2(L+1) \cos \frac{\pi(p+p')}{2(L+1)}}, \\
v_k^s(\alpha, \beta) &= \frac{2}{L+1} \left[\sin \frac{\pi q n_k}{L+1} \sin \frac{\pi q'(n_k-1)}{L+1} + \sin \frac{\pi q' n_k}{L+1} \sin \frac{\pi q(n_k-1)}{L+1} \right], \\
v_k^a(\alpha, \beta) &= \frac{2(-1)^{n_k}}{L+1} \left[\sin \frac{\pi q n_k}{L+1} \sin \frac{\pi q'(n_k-1)}{L+1} - \sin \frac{\pi q' n_k}{L+1} \sin \frac{\pi q(n_k-1)}{L+1} \right].
\end{aligned} \tag{49}$$

This close solution to the dimer model with an arbitrary number of monomers at fixed location can be formally used to get access to some informations about the general monomer-dimer model (see Appendix C).

3.2.2. Boundary monomers

Although the general problem remains in principle tractable, we can simplify it further by considering monomers on the boundary $m_i = L$ of the rectangle only, with the convention $n_i > n_j$ if $i > j$. When the

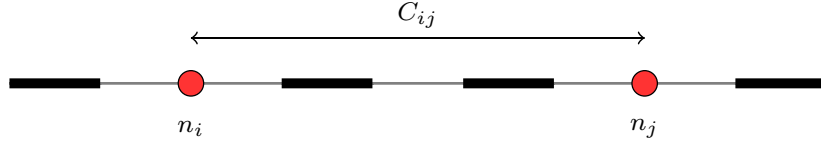


Figure 10: Configuration of 2 monomers on the boundary at the position n_i and n_j correlated by C_{ij} . This correlation decreases as the inverse of the distance and vanishes if n_i and n_j have the same parity.

monomers are on the boundaries of the domain, the off diagonal term V vanishes and the matrix W reduces to the matrix M (cf. Fig. 9(b)). In that case, the previous action contains no defect line term, only the couplings with fields remain and the problem can be transformed into a 1d system of particles on a chain (see Fig. 10). Using the previous Fourier transform for the c 's variables, the magnetic field term becomes

$$\begin{aligned}
\sum_{\mathbf{r}_i} c_{m_i, n_i} h_i &= \sum_{p, q=1}^L c_{pq} H_{pq}, \\
H_{pq} &= \sum_{\mathbf{r}_i} \frac{2i^{m_i+n_i}}{L+1} \sin \frac{\pi p m_i}{L+1} \sin \frac{\pi q n_i}{L+1} h_i.
\end{aligned} \tag{50}$$

Then the partition function can be integrated on the c_{mn} 's using the block partition (p, q) and we find that

$$Q_{2n}(\{\mathbf{r}_i\}) = Q_0 \int dh_1 \cdots dh_{2n} \exp S_H, \tag{51}$$

where

$$S_H = \sum_{p,q=1}^{L/2} \frac{it_x \cos \frac{\pi p}{L+1}}{2t_x^2 \cos^2 \frac{\pi p}{L+1} + 2t_y^2 \cos^2 \frac{\pi q}{L+1}} (H_{p-q}H_{-pq} + H_{pq}H_{-p-q}) \\ + \frac{it_y \cos \frac{\pi q}{L+1}}{2t_x^2 \cos^2 \frac{\pi p}{L+1} + 2t_y^2 \cos^2 \frac{\pi q}{L+1}} (H_{-pq}H_{-p-q} + H_{pq}H_{p-q}).$$

Grassmann fields H_{pq} has the following properties: $H_{-pq} = -H_{pq}$ and $H_{-p-q} = -H_{p-q}$. In that case, the first sum on the right hand side of the previous equation vanishes due to the anti-commuting property, and we can reduce the field-dependent action to one single sum

$$S_H = \sum'_{p,q=1} \frac{it_y \cos \frac{\pi q}{L+1}}{t_x^2 \cos^2 \frac{\pi p}{L+1} + t_y^2 \cos^2 \frac{\pi q}{L+1}} H_{pq}H_{p-q}, \quad (52)$$

where the prime symbol is meant for summation over half of the modes $p, q = 1 \dots L/2$. This action would vanish if all the n_i were for example even, since the Grassmann fields satisfy in this case $H_{pq}H_{p-q} = -H_{pq}^2 = 0$. In general, the field action can be rewritten as a quadratic form over the real-space fields h_i : $S_H = \sum_{i<j} C_{ij}h_ih_j$, where the elements of the matrix C are antisymmetric $C_{ij} = -C_{ji}$, and equal to

$$C_{ij} = \frac{4[(-1)^{n_i} - (-1)^{n_j}]}{(L+1)^2} \sum_{p,q=1}^{L/2} \frac{i^{1+n_i+n_j} t_y \cos \frac{\pi q}{L+1} \sin^2 \frac{\pi p}{L+1}}{t_x^2 \cos^2 \frac{\pi p}{L+1} + t_y^2 \cos^2 \frac{\pi q}{L+1}} \sin \frac{\pi q n_i}{L+1} \sin \frac{\pi q n_j}{L+1} \quad (53)$$

These elements are zero if n_i and n_j have the same parity and in general the integration over the field variables h_i leads directly to a pfaffian form for the partition function $Q_{2n}(\{\mathbf{r}_i\}) = Q_0(-1)^n \text{pf}(C)$. The $(-1)^n$ factor comes from the rearrangement of the measure $dh_1 \dots dh_{2n} = (-1)^n dh_{2n} \dots dh_1$, so that the $2n$ -function reads

$$\int \prod_{i=1}^{2n} dh_i \exp \left(- \sum_{i<j} C_{ij} h_i h_j \right) = \text{pf} C. \quad (54)$$

This sign could also be absorbed in the definition of matrix elements $C_{ij} \rightarrow -C_{ij}$. The resulting partition function is always positive with this definition. For example, if there are 2 monomers at the boundary, $\text{pf}(\hat{C}) = -C_{12}$, and 4 monomers⁹ leads to $\text{pf}(\hat{C}) = C_{12}C_{34} - C_{13}C_{24} + C_{14}C_{23}$ (cf. Fig. 11). We should notice that the expression Eq. (53) is an exact closed expression for the 2-point correlation between monomers on the boundary $m_i = m_j = L$, leading to an explicit result for the partition function with $2, 4, \dots, 2n$ monomers. We will show in a next section how to find the correlation between monomers on different (opposite or adjacent) boundaries of the lattice.

3.2.3. Single monomer on the boundary

We can recover the partition function for one monomer on the boundary using the previous analysis. In this case the size L has to be odd in order to accommodate for the presence of one single monomer. The action Eq. (119) is still valid, but the Fourier transform leads to a different block arrangement for the bulk

⁹As a straightforward application, the number of perfect matching with a monomer on each corner can be computed and the result is $Q_4^{\text{corner}} = \{1, 8, 784, 913952, 1211936774, \dots\}$

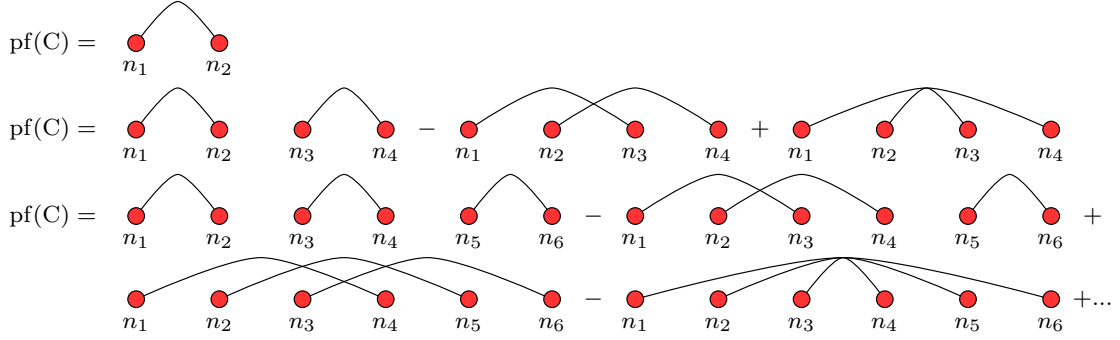


Figure 11: Diagrammatic representation of the pfaffian of C for 2, 4 and 6 monomers

terms Eq. (123) which are represented by the red zones in Fig. 12

$$\begin{aligned}
S_0 = & 2it_x \sum_{p,q \geq 1}^{\frac{1}{2}(L-1)} \cos \frac{\pi p}{L+1} (c_{pq}c_{-p-q} + c_{p-q}c_{-pq}) + 2it_x \sum_{p \geq 1}^{\frac{1}{2}(L-1)} \cos \frac{\pi p}{L+1} c_{p\frac{1}{2}(L+1)}c_{-p\frac{1}{2}(L+1)} \\
& + 2it_y \sum_{p,q \geq 1}^{\frac{1}{2}(L-1)} \cos \frac{\pi q}{L+1} (c_{pq}c_{p-q} + c_{-pq}c_{-p-q}) + 2it_y \sum_{q \geq 1}^{\frac{1}{2}(L-1)} \cos \frac{\pi q}{L+1} c_{\frac{1}{2}(L+1)q}c_{\frac{1}{2}(L+1)-q}.
\end{aligned}$$

S_0 contains Fourier modes that cover the Brillouin zone (see Fig. 12) except for term $c_{\frac{1}{2}(L+1)\frac{1}{2}(L+1)}$ which is located in the middle of the zone and not present in the sums Eq. (55). The integration over Grassmann variables c_{pq} is therefore zero in absence of coupling with this mode. Inserting a single monomer on the boundary at location $\mathbf{r} = (L, n)$ is equivalent, as previously demonstrated, to inserting a Grassmann field h and a field contribution $S_H = c_{Ln}h$ in the action, which can be expanded using Fourier transformation

$$\begin{aligned}
S_H &= \frac{2i^{L+n}}{L+1} \sum_{p,q} (-1)^{p+1} \sin \frac{\pi p}{L+1} \sin \frac{\pi qn}{L+1} c_{pq}h \\
&= \sum_{p,q} c_{pq}H_{pq}.
\end{aligned} \tag{55}$$

Since there is only one Grassmann field, all terms H_{pq} are only proportional to h , and therefore the quadratic form in Eq. (52) is zero. However one term contributes to the integration over $c_{\frac{1}{2}(L+1)\frac{1}{2}(L+1)}$, and corresponds to $c_{\frac{1}{2}(L+1)\frac{1}{2}(L+1)}H_{\frac{1}{2}(L+1)\frac{1}{2}(L+1)}$. After integration over the remaining c_{pq} and h variables, the partition function can then be factorized as

$$Q_1 = \frac{-2i^{n+1} \sin(\pi n/2)}{L+1} \prod_{p,q=1}^{\frac{1}{2}(L-1)} \left[4t_x^2 \cos^2 \frac{\pi p}{L+1} + 4t_y^2 \cos^2 \frac{\pi q}{L+1} \right] \prod_{p=1}^{\frac{1}{2}(L-1)} 2t_x \cos \frac{\pi p}{L+1} \prod_{q=1}^{\frac{1}{2}(L-1)} 2t_y \cos \frac{\pi q}{L+1}.$$

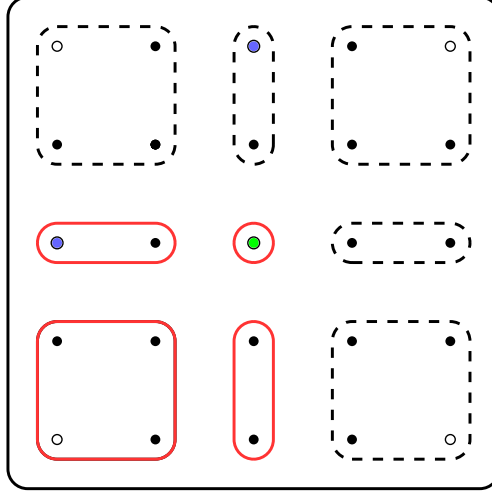


Figure 12: Block partition of the Fourier modes for L odd (here $L = 5$). There are 3 blocks of momenta (p, q) taken into account into the integration, plus one point (green dot) at location $(\frac{1}{2}(L+1), \frac{1}{2}(L+1))$. The first block of momenta (p, q) is represented in the red square for values $1 \leq p, q \leq \frac{1}{2}(L-1)$, with corresponding momenta $(\pm p, \pm q)$ (open dots). Then there are 2 additional lines of values $p = \frac{1}{2}(L-1)$ with $1 \leq q \leq \frac{1}{2}(L-1)/2$, and corresponding momentum $(\frac{1}{2}(L-1), -q)$, and $q = \frac{1}{2}(L-1)$ with $1 \leq p \leq \frac{1}{2}(L-1)/2$, and corresponding momentum $(-p, \frac{1}{2}(L-1))$, blue dots.

This result is consistent to the fact that a monomer can be put only at odd site locations. We can use the formula $\prod_{p=1}^{\frac{1}{2}(L-1)} 2 \cos(\frac{\pi p}{L+1}) = \sqrt{\frac{L+1}{2}}$, to simplify the previous expression and recover the Tzeng-Wu [136] solution

$$Q_1 = \prod_{p,q=1}^{\frac{1}{2}(L-1)} \left[4t_x^2 \cos^2 \frac{\pi p}{L+1} + 4t_y^2 \cos^2 \frac{\pi q}{L+1} \right] \times (t_x t_y)^{\frac{1}{2}(L-1)} \times [-i^{n+1} \sin(\pi n/2)]. \quad (56)$$

We can notice that the partition function with one monomer in a system of size $L \times L$ (L odd) is equal to the partition function without monomers on a lattice of size $L-1 \times L-1$. The probability is therefore constant for all location of the monomer, at even sites only, the last term in bracket being equal to zero (n odd) or unity (n even), proving that the monomer is fully delocalized on the boundary, unlike the bulk case where monomers are actually localized in a finite region of the domain [19, 75, 120].

3.3. Corner free energy and the central charge controversy

The study of finite size effects in statistical physics is a long standing and still active field of research [124]. *A fortiori* the possibility to solve a model in a non homogeneous geometry [64] is of prime interest for the understanding of behavior of physical systems in real situations. In the case of the dimer model on the rectangle with free boundary conditions, the system admit surfaces and corners, both of them play an important role in the behavior of the free energy in the thermodynamic limit. The exact solution of the close packing dimer model Eq. (10) on a even lattice ($M \times N = 2p$) allows for the study of the finite size effect of the free energy, and the finite size analysis has already been performed in the early time of the dimer model history [40].

Furthermore the exact solution Eq. (56) of the dimer model on a odd lattice ($M \times N = 2p+1$) with a monomer on a boundary allows for the study of the free energy in that case as well. Adding a finite number

of monomers in the dimer model is equivalent to a zero density of monomers in the continuum limit. Hence the presence of monomers does not give any contribution in the expression of the free energy, the only feature which plays a crucial role is the parity of the size of the lattice (even or odd). Because they are the simplest expressions of a even (odd) lattice with an even (odd) number of monomers, these two partition functions are sufficient to study all the details of the asymptotic limit of the free energy. In the following let us choose the square geometry $M = N = L$ for simplicity¹⁰. The free energy on a finite lattice of typical length L at criticality has the generic following form¹¹

$$\mathcal{F} = L^2 f_{\text{bulk}} + L f_{\text{surface}} + f_0 + a \log L + o\left(\frac{\log L}{L}\right). \quad (57)$$

The first term is the extensive contribution of the free energy, whereas the second one represents contribution from the lattice surface. In general, the coefficients f_{bulk} and f_{surface} are non-universal, but the coefficient f_0 is assumed to be universal, depending only on the shape and boundary conditions of the system. Universal properties of critical models appear in the subleading corrections and the value of f_0 is known to be simply related to the central charge c of the underlying conformal field theory. The study of statistical systems and their field theory representation in the presence of corners has been covered extensively, *e.g.* Ising and Potts model, loop model and percolation [73, 137, 100, 99], using various theoretical and numerical machinery. In two dimensions, as pointed out by Cardy and Peschel [25], the universal contribution to the free energy of a critical system in a domain with a corner with angle θ has been determined using the complex transformation

$$z \rightarrow z^{\theta/\pi} \quad (58)$$

which maps the upper half-plane onto the corner and looking at the holomorphic component of the stress-energy tensor in the corner. This mapping gives us the explicit form of the logarithmic contribution $\mathcal{F}_{\text{corner}} = a \log L$ in Eq. (57) and the result is $\frac{c}{24}(\frac{\theta}{\pi} - \frac{\pi}{\theta}) \log L$. It turns out that a additional complication arises because of the

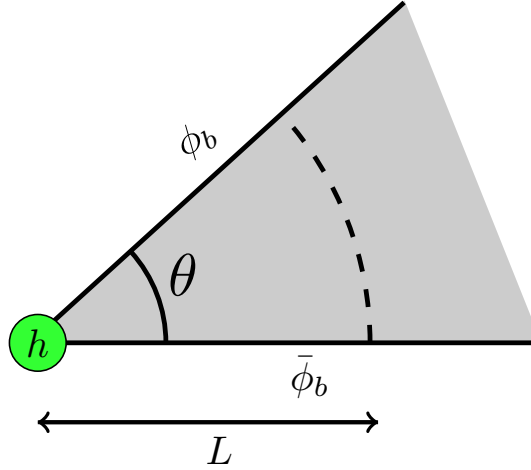


Figure 13: Corner of angle θ in a system of typical length L , in our situation $\theta = \pi/2$. The green dot symbolize a bcc operator of scaling dimension h_{bcc} which changes the value of the field either sides of the corner.

¹⁰The entire procedure can be extended to the case $M \neq N$ where the aspect ratio has to be taken into account, and no significant change appears [89].

¹¹The presentation here closely follows [131].

bcc operators [24] acting in the corners (*cf.* Fig. 13) as we saw in the section 2. In that particular case, the Cardy-Peschel contribution is slightly modified to taking into account this change of boundary conditions [90], and the logarithmic corner contribution becomes

$$\mathcal{F}_{\text{corner}} = \left[\frac{\pi}{\theta} h_{bcc} + \frac{c}{24} \left(\frac{\theta}{\pi} - \frac{\pi}{\theta} \right) \right] \log L \quad (59)$$

where h_{bcc} is the scaling dimension of the bcc operator. This bcc operator changes the boundary condition either sides of the corner in the height field representation. In their recent paper about corner free energy contribution in the free boundary conditions dimer model with one monomer at the boundary [69], the authors analyzed the asymptotic contribution of the four corners of the rectangular system without taking into account this bcc operator, ie taking $h_{bcc} = 0$ in the previous formula, and concluded that the central charge of the dimer model is $c = -2$. It is beyond the scope of this paper to enter into details in the wide area of conformal analysis of finite size effects (see [131] for more details), nor all the literature of $c = -2$ models, but just to pointing out the difference of result when one looks carefully at the bcc operator contribution in the corner free energy. In their paper, the authors found that the contribution of the four corners of the $L \times L$ (L odd) lattice is ¹²

$$\mathcal{F}_{\text{corner}} = \frac{1}{2} \log L. \quad (60)$$

The CFT formula Eq. (59) gives in the square geometry case ($\theta = \pi/2$)

$$\mathcal{F}_{\text{corner}} = \left[\frac{-c}{4} + 2(h_{bcc}^{(1)} + h_{bcc}^{(2)} + h_{bcc}^{(3)} + h_{bcc}^{(4)}) \right] \log L, \quad (61)$$

where $h_{bcc}^{(\nu=1..4)}$ are the dimensions of the four bcc operators living on the corners. Taking $h_{bcc} = 0$ leads *de facto* to $c = -2$, suggesting that the dimer model may be a logarithmic CFT (LCFT) [72, 123, 125]. This statement is also based on the mapping of the dimer model to the spanning tree model [134] and, equivalently, to the Abelian sandpile model [107] which both belong to a $c = -2$ LCFT, facts which we do not dispute here. The problem with this analysis is the oversight of the bcc operators acting on the corners. We know that the partition function with one monomer on the boundary does not depend of the location of the monomer, then let us choose to put it on the corner for simplicity. In this following case, the height field is shifted either sides of the corner, precisely we obtain the value $h = (.0101..)$ in one side and $h = (..-2-3-2-3..)$ on the other side (see Fig. 14), making a height shift of $\Delta\phi_b = 3\pi/2$, therefore using Eq. (27), the dimension of the bcc operator on the corner is $9/32$ (which is actually the dimension of the original bcc plus the dimension of the corner monomer operator as we will see in the next section). The three other corners induce a height shift of $\pi/2$, thus the dimension of the bcc operators is $1/32$ as in the case where monomer are absent. Finally we find

$$\mathcal{F}_{\text{corner}} = \left[\frac{-c}{4} + 2 \left(\frac{9}{32} + \frac{1}{32} + \frac{1}{32} + \frac{1}{32} \right) \right] \log L. \quad (62)$$

The comparison with the asymptotic result Eq. (60) gives us the value of the central charge of the free bosonic field theory, *i.e.* $c = 1$ ¹³. Obviously this result seems completely natural in the height mapping framework or in the free complex fermion representation of the dimer model Eq. (37), nonetheless the presence of bcc

¹²*cf.* [69] for details of the asymptotic calculation.

¹³One can notice that the same result holds if the monomer is somewhere on the boundary but not at the corner, in that case, there is five bcc operators, four on each corners of dimension $1/32$ and another responsible for the shift at the surface with dimension $1/2$ then using Eq. (59)

$$\mathcal{F}_{\text{corner}} = \left[\frac{-c}{4} + \frac{1}{2} + 2 \left(\frac{1}{32} + \frac{1}{32} + \frac{1}{32} + \frac{1}{32} \right) \right] \log L = \frac{1}{2} \log L, \quad (63)$$

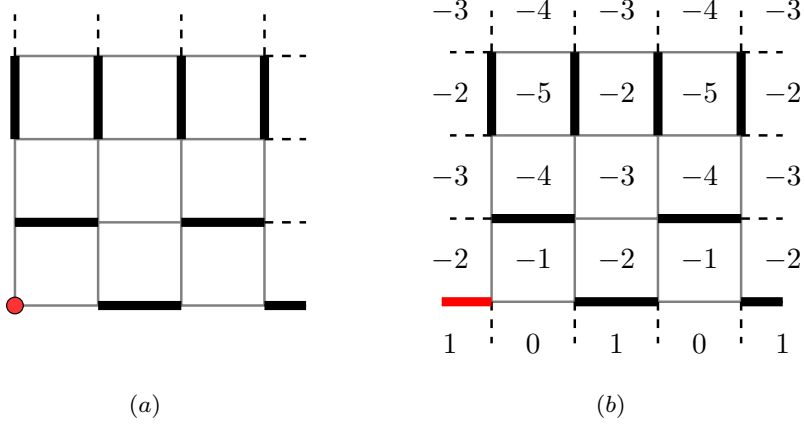


Figure 14: (a) Representation of the corner region of a lattice with one monomer at the corner. (b) The monomer can be represented by a virtual red dimer which gives the same configurations. The different values of the height field either sides of the corner are induced by a bcc operator of scaling dimension $9/32$.

operators acting on the corners has never been extensively studied in this context, leading to misinterpretation of asymptotic results and thus to a different value of the central charge of the theory. In the pure dimer situation Eq. (10), the four bcc operators has dimension $1/32$, we claim that the corner free energy should be equal to

$$\mathcal{F}_{\text{corner}} = \left[\frac{-1}{4} + 2(4h_{bcc}) \right] \log L = 0. \quad (64)$$

This result nicely agrees with the literature, where no corner free energy term has never been found in the free boundary conditions close packed dimer model, neither theoretically [20] nor numerically [95], strengthening our analysis¹⁴. Previously another type of finite size effect analysis [72] has been performed for the close packing dimer model on a strip with periodic and free boundary conditions, and it has been shown that the result depends strongly on the parity of the length of the strip as it should be, and the notion of effective central charge has to be introduced [67]. Though the comparison with the CFT result gives the value $c = -2$, we claim here that the analysis of the free energy in the height mapping formulation of boundary conditions, leads again to $c = 1$. In the following section, we shall compute analytically correlation functions between monomers where boundary fields has to be properly interpreted and we will show that the exact solution fully agrees with this theory, reinforcing the present result about the significance of these bcc operators. Finally we conclude, that the free bosonic formulation of the dimer model allows for the complete study and interpretation of finite size effects in a CFT context, and unified all the results known about this very simple but not trivial model.

4. Exact correlations: discrete and continuous cases

In this section, detailed computations of correlations are performed in terms of disorder operators. A particular attention will be paid to the special case of boundary monomers, where a closed-form expression is obtained, valid for any of the four boundaries of the rectangle. Then, numerical evaluations of the exact pfaffian

in accordance with the fact that the partition function with one boundary monomer does not depend of its location.

¹⁴The same analysis can be done for the same model with periodic boundary conditions in one direction and free in the other, leading to the same conclusion about the central charge.

solution are done and diverse monomer and dimer correlations are obtained for bulk, surface and corner cases, leading to the whole set of scaling dimensions which can be compared to the bosonic theory with $g = 1/4\pi$.

4.1. Fermion correlations and disorder operators

The addition of monomers in the dimer model is therefore equivalent to inserting a magnetic field h_i at points \mathbf{r}_i , as well as a line of defect running from the monomer position to the right boundary $m = L$. If two monomers have the same ordinate $n_i = n_j$, the line of defects will only run between the two monomers and will not reach the boundary. This can be viewed as an operator acting on the links crossed by the line and running from a point on the dual lattice to the boundary on the right-hand side. More specifically, we can express the correlation functions, after integration over the fermionic magnetic fields h_i , as an average over composite fields

$$\begin{aligned} \frac{Q_{2n}(\{\mathbf{r}_i\})}{Q_0} &= \left\langle \prod_{\{\mathbf{r}_i\}} c_{m_i n_i} \exp \left(2t_y \sum_{m=m_i+1}^L (-1)^{m+1} c_{m n_{i-1}} c_{m n_i} \right) \right\rangle_0 \\ &= \left\langle \prod_{\{\mathbf{r}_i\}} c_{m_i n_i} \mu(\mathbf{r}_i + \mathbf{e}_4) \right\rangle_0 \\ &= \left\langle \prod_{\{\mathbf{r}_i\}} \Psi_4(\mathbf{r}_i) \right\rangle_0, \end{aligned} \quad (65)$$

where $\mu(\mathbf{r} + \mathbf{e}_4)$ is a fermionic disorder operator, whose role is to change the sign of the vertical links across its path starting from vector $\mathbf{r} + \mathbf{e}_4$ on the dual lattice (*cf.* [5] for details). The integration $\langle \cdots \rangle_0$ is performed relatively to the action S_0 . Likewise the Kasteleyn theory, where disorder lines are absent on the boundary and where correlations between monomers correspond to correlations between Grassmann variables Eq. (15), here the correlation between monomers on the boundaries are exactly correlation functions between the fermionic fields

$$\frac{Q_{2n}(\{\mathbf{r}_i\})}{Q_0} = \left\langle \prod_{\{\mathbf{r}_i\}} c_{m_i n_i} \right\rangle_0. \quad (66)$$

This result about monomer correlations written in terms of disorder operators is the fermionized version of the Coulomb gas framework, where monomers act like dual magnetic charges which create a dislocation of the height field and correspond to the vertex operator of the corresponding bosonic field theory.

4.2. Perturbative expansion of the 2-point function

In the case where the monomers are on the boundaries, we were able to compute exactly the 2-point correlation function Eq. (53) in the discrete case. In the bulk case, the things are much more complicated and an exact closed-form expression on the discrete level seems out of reach. Nevertheless, a perturbative expansion can be performed to evaluate the pfaffian expression of the correlation function. We start from the exact pfaffian expression of matrix C

$$C_{ij} = \Lambda_{i,\alpha}^\mu (W^{-1})_{\alpha\beta}^{\mu\nu} \Lambda_{j,\beta}^\nu. \quad (67)$$

The inverse matrix W^{-1} can be computed using formally the expansion

$$W^{-1} = (M + V)^{-1} = M^{-1} - M^{-1} V M^{-1} + \mathcal{O}(V^2). \quad (68)$$

In particular it is convenient to write the inverse matrix M^{-1} as

$$M_{\alpha}^{-1} = \bar{a}_x(p)\Gamma_x + \bar{a}_y(q)\Gamma_y, \quad (69)$$

with

$$\begin{aligned} \bar{a}_x(p) &= -\frac{a_x(p)}{a_x(p)^2 + a_y(q)^2} \\ \bar{a}_y(q) &= -\frac{a_y(q)}{[a_x(p)^2 + a_y(q)^2]}. \end{aligned} \quad (70)$$

In the following we will consider only the first of this expansion

$$\begin{aligned} C_{ij} &= \sum_{\alpha, \beta} \langle \mathbf{\Lambda}_{i, \alpha} | W_{\alpha\beta}^{-1} | \mathbf{\Lambda}_{j, \beta} \rangle = \sum_{\alpha} \sum_{\mu} r_i(\alpha) \bar{a}_{\mu}(\alpha) r_j(\alpha) \langle \mathbf{\Lambda}_i | \Gamma_{\mu} | \mathbf{\Lambda}_j \rangle \\ &\quad - \sum_{\alpha, \beta} \sum_{\mu, \nu} \sum_{\mathbf{r}_k} \sum_{c, c'=\{a, s\}} r_i(\alpha) \bar{a}_{\mu}(\alpha) u_k^c(\alpha, \beta) v_k^{c'}(\alpha, \beta) \bar{a}_{\nu}(\beta) r_j(\beta) \langle \mathbf{\Lambda}_i | \Gamma_{\mu} \Gamma_{cc'} \Gamma_{\nu} | \mathbf{\Lambda}_j \rangle + \dots \\ &= C_{ij}^{(0)} + C_{ij}^{(1)} + \dots \end{aligned} \quad (71)$$

The structure of this expansion make possible a further diagrammatic expansion of the quantities C_{ij} as a series of term $C_{ij}^{(k)}$, with $k \geq 0$. The first term $C_{ij}^{(0)}$ has symmetry factors

$$\begin{aligned} \langle \mathbf{\Lambda}_i | \Gamma_x | \mathbf{\Lambda}_j \rangle &= \overbrace{i^{m_i+n_i+m_j+n_j}}^{c_{ij}} \overbrace{[(-1)^{m_i} - (-1)^{m_j}] [(-1)^{n_i} + (-1)^{n_j}]}^{\gamma_{ij}^{(1)}} := c_{ij} \gamma_{ij}^{(1)}, \\ \langle \mathbf{\Lambda}_i | \Gamma_y | \mathbf{\Lambda}_j \rangle &= \overbrace{i^{m_i+n_i+m_j+n_j}}^{c_{ij}} \overbrace{[1 + (-1)^{m_i+m_j}] [(-1)^{n_j} - (-1)^{n_i}]}^{\gamma_{ij}^{(2)}} := c_{ij} \gamma_{ij}^{(2)}. \end{aligned} \quad (72)$$

It is easy to see that $\langle \mathbf{\Lambda}_i | \Gamma_x | \mathbf{\Lambda}_j \rangle = 0$ for monomers on the boundary or on the same column, when $m_i = m_j$. *A contrario*, for pairs of monomers on the same line $n_i = n_j$, we have $\langle \mathbf{\Lambda}_i | \Gamma_y | \mathbf{\Lambda}_j \rangle = 0$. The first term $C_{ij}^{(0)}$ can be expressed in the discrete case as

$$\begin{aligned} C_{ij}^{(0)}(L) &= \frac{2c_{ij}}{(L+1)^2} \sum_{p, q=1}^{L/2} \left\{ \frac{\gamma_{ij}^{(1)} t_x \cos \frac{\pi p}{L+1}}{t_x^2 \cos^2 \frac{\pi p}{L+1} + t_y^2 \cos^2 \frac{\pi q}{L+1}} + \frac{\gamma_{ij}^{(2)} t_y \cos \frac{\pi q}{L+1}}{t_x^2 \cos^2 \frac{\pi p}{L+1} + t_y^2 \cos^2 \frac{\pi q}{L+1}} \right\} \\ &\quad \times \sin \frac{\pi p m_i}{L+1} \sin \frac{\pi p m_j}{L+1} \sin \frac{\pi q n_i}{L+1} \sin \frac{\pi q n_j}{L+1}. \end{aligned} \quad (73)$$

This expression is valid for 2 monomers on any of the four boundaries of the lattice, and is identical, when $m_i = m_j = L$, to expression obtained for the same ($m_i = n_i = L$) boundary case Eq. (53). Indeed the first order of the expansion Eq. (68) is valid only on the boundaries where the matrix W is actually equal to the matrix M . One could demonstrate that this 2-point correlation is actually exact $C_{ij}^{(0)} = C_{ij}$ for boundary monomers because of the cancelation of higher terms in the perturbative expansion, accordingly the expression Eq. (73) is a general exact result for any positions anywhere on the four boundaries. Therefore, it will be very efficient to use this exact closed-form to evaluate scaling behaviors of correlation functions between monomers on the surface and at the corners. This present perturbative expansion can be performed to the next leading order to evaluate bulk correlations, and will be detailed elsewhere.

4.3. Scaling behavior of monomer correlation functions

Here, we shall analyze monomer-monomer correlation functions using our pfaffian solution detailed previously and compared to the Coulomb gas interpretation of the dimer model. As we saw in section 2, the dimer model on a rectangular geometry admit a *bcc* operator on every of the four corners, and it has to be taken into account for the analysis of the scaling dimension operators, in particular for corner correlations. Indeed in the case of monomers deep in the bulk¹⁵ or deep in the surface¹⁶, the scaling dimensions are respectively $x_b^{(m)} = 1/4$ and $x_s^{(m)} = 1/2$, leading to the following scaling of correlation functions (see Fig. 16(a))

$$\text{monomer correlations} \rightarrow \begin{cases} \text{bulk-bulk behavior} \rightarrow C(L) \sim L^{-2x_b^{(m)}} \sim L^{-1/2} \\ \text{surface-surface behavior} \rightarrow C(L) \sim L^{-2x_s^{(m)}} \sim L^{-1} \\ \text{bulk-surface behavior} \rightarrow C(L) \sim L^{-x_s^{(m)}-x_b^{(m)}} \sim L^{-3/4}. \end{cases} \quad (74)$$

These known results are in perfect agreement with our exact solution (*cf.* Fig. 15) where we fixed the positions of two monomers for increasing system size L (all the correlations are measured for $t_x = t_y = 1$). The behaviors

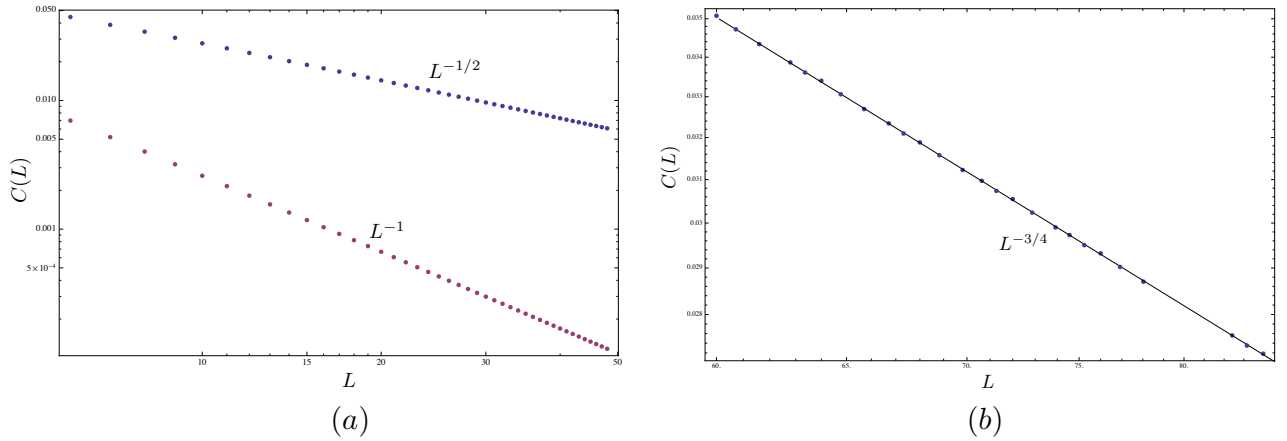


Figure 15: (a) Bulk-bulk and surface-surface correlation functions. (b) Bulk-surface monomer correlation functions

of bulk and surface monomer correlation functions had already been studied in several papers, and the scaling dimensions are related to the scaling dimensions of operators of the $2d$ Ising model *via* the expression of monomer-monomer correlations as spin-spin correlations [6]. At present, we consider the effects of corners in our system, which seems to be more difficult to consider as we have seen for the corner contribution to the free energy. Fortunately conformal invariance predicts a relation for the scaling dimension of an operator in the vicinity of a corner of an angle θ in terms of the scaling dimension of the same operator on the surface [25]

$$x_c = \frac{\pi}{\theta} x_s. \quad (75)$$

If we believe in this formula, we should obtain the value $x_c^{(m)} = 1$ for $\theta = \pi/2$, which leads to the behavior $C(L) \sim L^{-2}$ for corner-corner correlation functions. This result contradicts our exact evaluation, where the exponent seems to change according to the exact location of the monomers (see Fig. 16(b) and Fig. 18), and

¹⁵far from surfaces and corners.

¹⁶far from corners.

where three different cases arise. Unlike the surface and bulk cases where the scaling dimensions are uniquely defined, the corner scaling dimension appears to be less trivial to analyze, and the influence of the bcc operators has to be carefully taking into account. We should mention that the same kind of analysis has been done for the Ising model, where the magnetization was measured for various spins close to a corner [116]. We saw previously

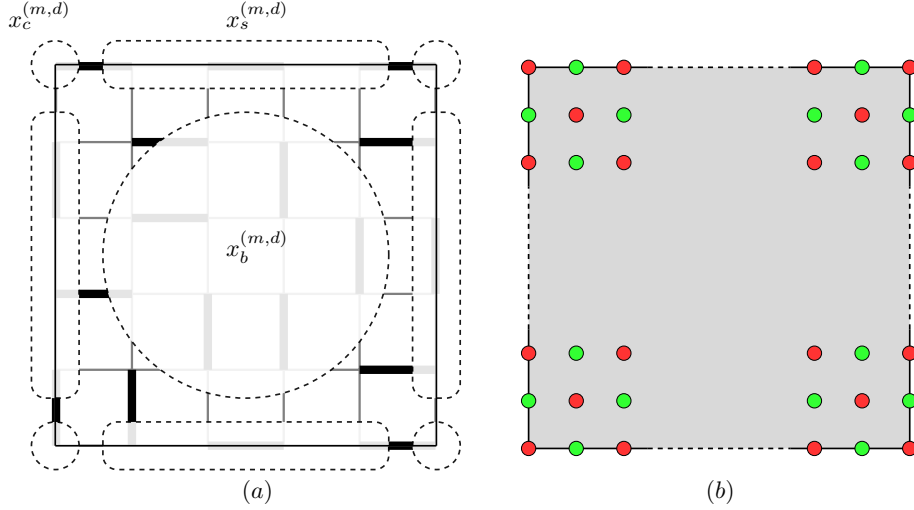


Figure 16: (a) Bulk, surface and corner decomposition of the square. (b) Representation of the values of the scaling dimensions of monomer operators close to the corners. Monomers on red sites have dimension 1/2 while monomers on green sites have dimension 3/2. Let us notice that this distinction is different from the even/odd sublattice distinction because opposite sublattice sites may have the same dimension and *vice versa*.

Eq. (61), that bcc operators add a logarithm term in the expression of the free energy \mathcal{F} of a rectangular system, then this contribution to the partition function scale as

$$Q(L) \sim L^{-2(h_{bcc}^{(1)} + h_{bcc}^{(2)} + h_{bcc}^{(3)} + h_{bcc}^{(4)})} = L^{-2(1/32 + 1/32 + 1/32 + 1/32)}. \quad (76)$$

Indeed putting two monomers exactly on the corner of the same boundary (see Fig. 18(a)) is equivalent to a height shift of value $3\pi/2$ in each corner. This height shift is induced by an operator of dimension $9/32$, leading to the following behavior of the partition function with the two monomers

$$Q_2(L) \sim L^{-2(1/32 + 1/32 + 9/32 + 9/32)}. \quad (77)$$

Here the correlation function scale then as $C(L) = Q_2 Q_0^{-1} \sim L^{-1}$ leading to the value $x_c^{(m)} = 1/2$ of the monomer corner scaling dimension. Nevertheless, if one choose the diagonal corners (see Fig. 18(b)), we place a monomer on the first corner which is again equivalent to the insertion of a bcc operator of dimension $9/32$ (see Fig. 14) and the other one on a neighboring site of the other corner which is equivalent to the insertion of a bcc operator of dimension $25/32$ (see Fig. 17), we found the behavior $C(L) \sim L^{-2}$. Finally, if both of the two monomers are on a neighboring site of a corner (see Fig. 18(c)), then the correlation function is $C(L) \sim L^{-3}$. This three different situations are summarized in Fig. 18, showing that our exact computations are in perfect agreements with Coulomb gas predictions for the behavior of correlation functions in the vicinity of a corner. A more general statement is that the monomer scaling dimension near a corner depends crucially of the sublattice considered as explained in Fig. 16(b). This phenomena leads to two different values of the scaling dimension for corner monomers $x_c^{(m)} = 1/2$ or $3/2$ which is in agreement with the CFT formula Eq. (75) in average when lattice effects are forgotten. A general study of the finite size behavior of correlation functions can be performed

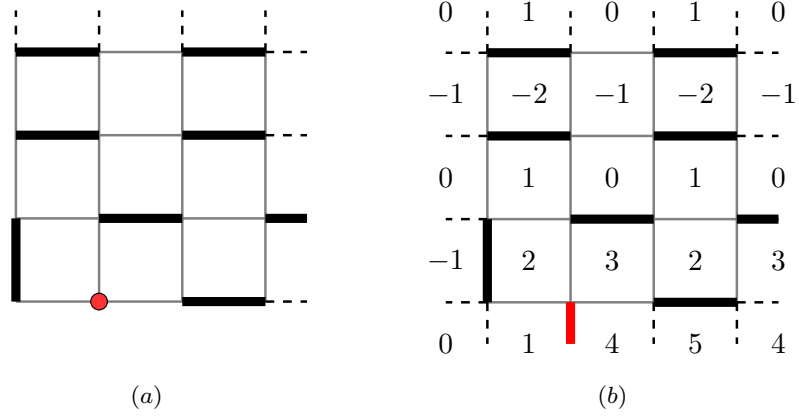


Figure 17: (a) Representation of the corner region of a lattice with one monomer at the corner. (b) The monomer can be represented by a virtual red dimer which gives the same configurations. The different values of the height field either sides of the corner are induced by a *bcc* operator of scaling dimension $25/32$.

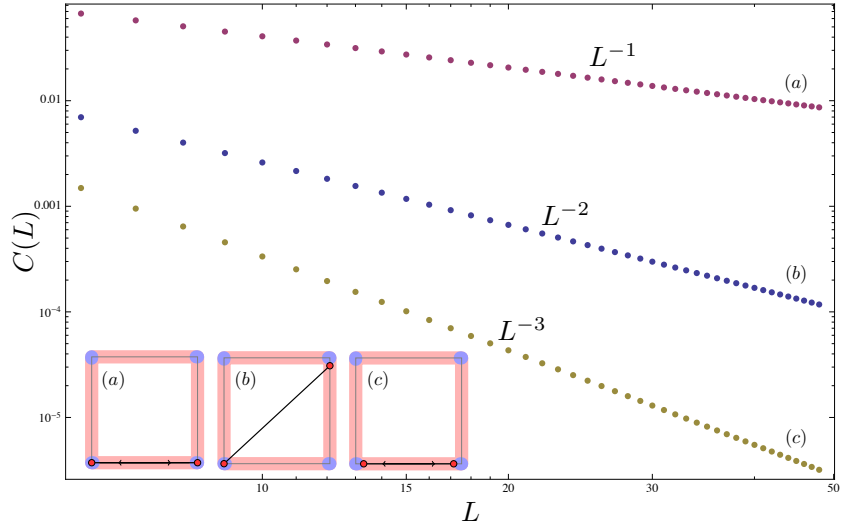


Figure 18: Corner-Corner in the three different situations pictured on the graphical representation: (a) the two monomers exactly on the corners. (b) One monomer on one corner and the other one on a adjacent site of another corner. (c) Two monomers on a adjacent sites of opposite corners.

as well, leading to the following scaling ansatz

$$C(r_1, r_2, L) = |r_1 - r_2|^{-x_1 - x_2} \Phi(|r_1 - r_2|^{-1} L), \quad (78)$$

where r_1 and r_2 are the positions of the two monomers, with respective scaling dimensions x_1 and x_2 . The scaling function $\Phi(u)$ depends on the position of the operators and goes to a constant in the scaling limit $u \rightarrow \infty$ (see Fig. 19). The translation and rotational invariance has been checked analytically and numerically, and in

the following we will use $|r_1 - r_2| = r$

$$C(r) \sim r^{-x_1 - x_2}. \quad (79)$$

This scaling behavior is shown for bulk-bulk and surface-surface correlations in Fig. 19. The exact form of

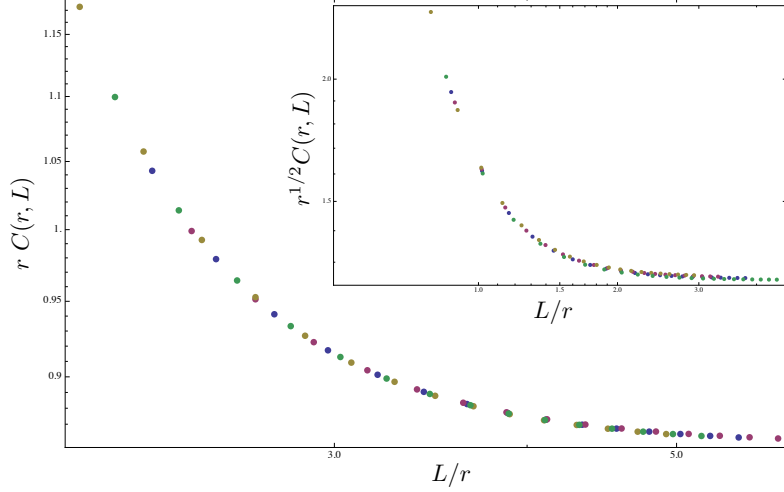


Figure 19: Finite size scaling of monomer surface-surface and bulk-bulk (inset) correlation functions in log-log scale for $L = 100, 200, 300, 400$. The surface correlations are measured far from the corners and the bulk correlations are measured far from boundaries and corners.

the scaling function Ψ seems hard to obtain explicitly, but at least for boundary and corner cases it should be possible to extract the scaling behaviors using the expression Eq. (73) of exact correlation functions. We let this question for a future work and we hope that comparisons with CFT predictions can be made.

4.4. Scaling behavior of dimer correlation functions

As we have shown in section 2 of this article, the bulk correlation between a dimer covering the two neighboring sites i and j and another dimer covering the two neighboring sites m and n can be computed in the Kasteleyn-Fisher-Temperley pfaffian formalism leading to a behavior in L^{-2} in the thermodynamic limit. Let us note $D(L)$ this quantity. In the Coulomb gas approach, dimers are interpreted as electric charges with scaling dimensions $x_b^{(d)} := x_{\frac{1}{4\pi}}(1, 0)$, the result for dimer-dimer correlations gives us the value $x_b^{(d)} = 1$. Actually it is straightforward to study dimer correlations here. Indeed a dimer can be seen as two neighboring monomers, thus a dimer-dimer correlation is simply a 4-point monomer-monomer correlation, which can be evaluated with our solution. In the following, one shows how to construct the dimer-dimer correlation in the boundary case, for the bulk case the situation is essentially the same but expressions are less convenient. Explicitly the correlation between two dimers at position (r_i, r_j) and (r_m, r_n) is

$$Q_4(r_i, r_j, r_m, r_n)Q_0^{-1} = C_{ij}C_{mn} - C_{im}C_{jn} + C_{in}C_{jm}. \quad (80)$$

If we choose that r_i and r_m are on the same sublattice (then r_j and r_n are on the other one), a straightforward consequence is that the second term $C_{im}C_{jn}$ vanishes, moreover the first term $C_{ij}C_{mn}$ tends to a constant in the thermodynamic limit in such way that we can define the dimer-dimer correlation function as

$$Q_4(r_i, r_j, r_m, r_n)Q_0^{-1} - C_{ij}C_{mn} = C_{in}C_{jm} \sim D(L). \quad (81)$$

In this way, all the configurations of dimer correlations are available, and all the scaling dimensions of electric charges (bulk, surface, corner) may be analyzed *stricto sensu* and compared with the Coulomb gas theory. We can show that the well known bulk behavior is recovered very precisely, furthermore, surface and corner correlations may be examined as well leading to the following behaviors

$$\text{dimer correlations} \rightarrow \begin{cases} \text{bulk-bulk behavior} \rightarrow D(L) \sim L^{-2x_b^{(d)}} \sim L^{-2}, \\ \text{surface-surface behavior} \rightarrow D(L) \sim L^{-2x_s^{(d)}} \sim L^{-2}, \\ \text{corner-corner behavior} \rightarrow D(L) \sim L^{-2x_c^{(d)}} \sim L^{-4}. \end{cases} \quad (82)$$

Unlike monomer correlations, dimer correlations are much easier to interpret in the Coulomb gas framework. Indeed, the absence of additional change of boundary conditions¹⁷ in the partition function allows for a direct determination of dimer scaling dimensions. The particular form of dimer correlations Eq. (81) predicts that $x_s^{(d)} = 2x_s^{(m)} = 1$ ¹⁸ and $x_c^{(d)} = x_{c+}^{(m)} + x_{c-}^{(m)} = 2$ ¹⁹. We notice here that the formula Eq. (75) checked out in that case. A careful and detailed study of surface and corner operators has to be performed to unravel this point. The scaling form of correlation functions Eq. (78) holds in the dimer case as well, using the dimer scaling dimensions (see Table 2). The solution presented in this article can be also used to calculate more complex

scaling dimension ($g_{\text{free}} = 1/4\pi$)	bulk	surface	corner
$x^{(d)}$	1	1	2
$x^{(m)}$	1/4	1/2	1/2 or 3/2

Table 2: Bulk, surface and corner values of dimer and monomer scaling dimensions for the free ($g_{\text{free}} = 1/4\pi$) fixed point. The corner monomer scaling dimension depends of its exact location.

correlation functions, combining dimer and monomer scaling dimensions. *A posteriori*, more complicated object like trimers, quadrimers or more generally, string of k neighboring monomers (k -mer) can be studied as well, which correspond to various charged particles in the Coulomb gas formalism.

5. About some combinatorial properties

In this section, one shows a curious combinatorial analogy between the partition function of the close packing dimer model on a $L \times L$ square lattice with open boundary conditions, and the same partition function with boundary monomers. One start reminding some properties of the pure dimer model partition function, and we show, thanks to our exact calculation of the partition function with $2n$ monomers, that this analogy can be understood and demonstrated. Hereinafter, the Boltzmann weights t_x and t_y are taken to be the unity in such way that the partition function is exactly equal to the perfect matching number. All the results presented in this section has been checked with depth-first [101] algorithms up to size $L = 10$. For bigger sizes, Monte-carlo simulations [102] or transfer matrix calculation [104] has to be implemented.

¹⁷Of course the four corner *bcc*'s with dimension $1/32$ are still present but do not play any role in dimer-dimer correlation functions.

¹⁸Let us notice that the fact that $x_b^{(d)} = x_s^{(d)}$ is a pure coincidence.

¹⁹A dimer in the corner is formed by two neighboring monomers with dimension $x_{c+}^{(m)}$ and $x_{c-}^{(m)}$.

5.1. Partition function without monomers

The partition function of the pure dimer model on a $M \times N$ lattice with open boundary conditions is

$$Q_0(M, N) = \prod_{p=1}^{M/2} \prod_{q=1}^{N/2} \left[4 \cos^2 \frac{\pi p}{M+1} + 4 \cos^2 \frac{\pi q}{N+1} \right], \quad (83)$$

which can be written for the special case of the square geometry $M = N = L$

$$Q_0(L) = 2^{L/2} \cdot g_{L/2}^2 \quad (84)$$

where $g_{L/2}$ is a number sequence (OEIS A065072)²⁰ equal, for $L = 2, 4, 6, 8, 10, 12, 14, \dots$, to

$$g_{L/2} = \{1, 3, 29, 901, 89893, 28793575, 29607089625, \dots\}.$$

The resulting sequence for the partition function is then (OEIS A004003) for $L = 2, 4, 6, 8, 10, 12, 14$

$$Q_0 = \{2, 36, 6728, 12988816, 258584046368, 53060477521960000, 112202208776036178000000, \dots\}.$$

For example, the number of configurations of dimers on the chessboard ($L = 8$) is $Q_0(8) = 2^4 g_4^2 = 2^4 \times 901^2 = 12988816$ as previously noticed by Fisher [41]. Another observation is that the number of configuration on the square $L \times L$ is always even. It is less trivial to notice that $\{g_p\}$ is a sequence of odd number satisfying the relation [77]

$$\begin{aligned} g_p &= p + 1 \pmod{32} \quad \text{if } p \text{ even} \\ &= (-1)^{(p-1)/2} \times p \pmod{32} \quad \text{if } p \text{ odd.} \end{aligned} \quad (85)$$

The exact solution of the dimer model with one boundary monomer allows for the same kind of number theory analysis (*cf.* [97] for details). The aim of the following sections is to look in more details at the form of the partition function of a dimer model of on a $L \times L$ square (L even) lattice with $2n$ monomers. One allows the $2n$ monomers to be anywhere on the four boundaries of the square (see Fig. 20).

5.2. Partition function with two boundary monomers

We saw previously that the expression of this partition function Q_{2n} is related to the pure dimer model Q_0 by the formula

$$Q_{2n} = Q_0 \cdot \text{pf}(C), \quad (86)$$

where the size of the matrix C depend of the number of monomers. Previously, the partition Q_0 has been shown to possess a remarkable expression Eq. (84) and we would like to determine whether or not, the partition function Q_{2n} admit the same kind of properties. In the case of two monomers anywhere on the boundaries, we saw that $W = M$ and then the expression Eq. (86) reduces to

$$Q_2 = Q_0 \cdot C_{ij}. \quad (87)$$

²⁰The On-Line Encyclopedia of Integer Sequences <https://oeis.org/>

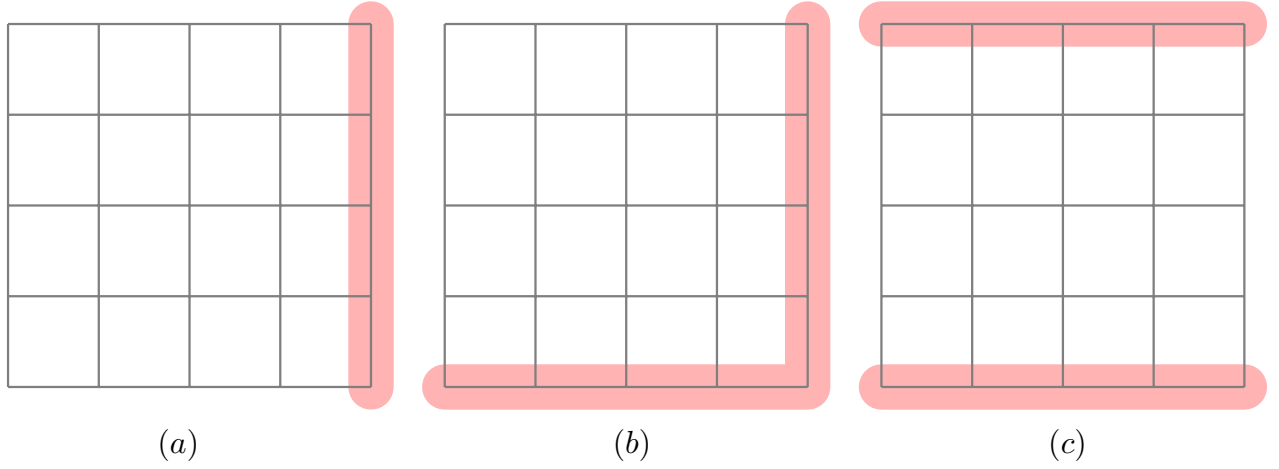


Figure 20: The three different possibilities of two monomer's location. (a) on a same boundary (b) on adjacent boundaries or (c) on opposite boundaries.

5.2.1. Inline boundary monomers

Initially, we choose to restrict the monomers to live on the same boundary $m_i = m_j = L$ with $n_i, n_j \in [1, L]$ (cf. Fig. 20(a)). In that particular situation the matrix elements C_{ij} take the following form Eq. (53)

$$C_{ij} = R_{ij} \sqrt{\frac{2}{L+1}} \sum_{p,q=1}^{L/2} \frac{i^{1+n_i+n_j} \cos \frac{\pi q}{L+1} \sin^2 \frac{\pi p}{L+1}}{\cos^2 \frac{\pi p}{L+1} + \cos^2 \frac{\pi q}{L+1}} \sin \frac{\pi q n_i}{L+1} \sin \frac{\pi q n_j}{L+1} \quad (88)$$

where

$$\begin{aligned} R_{ij} &= \pm 2 \text{ if } n_i \in \mathbb{Z}_{2p}(\mathbb{Z}_{2p+1}) \text{ and } n_j \in \mathbb{Z}_{2p}(\mathbb{Z}_{2p+1}) \\ &= 0 \text{ if } n_i \in \mathbb{Z}_{2p} \text{ and } n_j \in \mathbb{Z}_{2p+1} \text{ or conversely.} \end{aligned} \quad (89)$$

In table 3, we evaluate this expression using MATHEMATICA[®], restricting one monomer to be in $n_j = 1$ and the second to be between 1 to L for several system sizes. One can observe that there is a curious relation between

$C_{ij}(L)$	4	6	8	10	12	14
$(1, 1), (2, 1)$	1/2	1/2	1/2	1/2	1/2	1/2
$(1, 1), (4, 1)$	1/3	9/29	275/901	27293/89893	8724245/28793575	8962349805/29607089625
$(1, 1), (6, 1)$.	7/29	199/901	19279/89893	6103405/28793575	6242309595/29607089625
$(1, 1), (8, 1)$.	.	169/901	15395/89893	4750015/28793575	4800013155/29607089625
$(1, 1), (10, 1)$.	.	.	13761/89893	4036195/28793575	3979640565/29607089625
$(1, 1), (12, 1)$	3721985/28793575	3520442385/29607089625
$(1, 1), (14, 1)$	3311911215/29607089625
$g_{L/2}$	3	29	901	89893	28793575	29607089625

Table 3: Correlation function C_{ij} for a boundary monomer ($m_i = m_j = L$) fixed on the first site $n_j = 1$ as function of the ordinate n_i for several system sizes L (see Fig. 20(a)). The value of C_{ij} where the two monomers are on the corner $(1, 1), (2, 1)$ is always equal to 1/2, because it is equivalent to force a dimer to be on the corner and then split the number of configuration by two. Bottom line: Values of the sequence g_L for $L = 4..14$.

the expression C_{ij} and the sequence $g_{L/2}$ present in the partition function Q_0 , more precisely one can deduce a proportionality relation

$$C_{ij}(L) \propto g_{L/2}^{-1}, \quad (90)$$

which appears to be valid for all system sizes L in the case of inline monomers.

5.2.2. General case

The general expression of the matrix elements of the correlations between boundary monomers Eq. (73), valid in all the geometries of Fig. 20 can be written as

$$C_{ij} = \frac{2c_{ij}}{(L+1)^2} \sum_{p,q=1}^{L/2} \left\{ \frac{\gamma_{ij}^{(1)} t_x \cos \frac{\pi p}{L+1}}{t_x^2 \cos^2 \frac{\pi p}{L+1} + t_y^2 \cos^2 \frac{\pi q}{L+1}} + \frac{\gamma_{ij}^{(2)} t_y \cos \frac{\pi q}{L+1}}{t_x^2 \cos^2 \frac{\pi p}{L+1} + t_y^2 \cos^2 \frac{\pi q}{L+1}} \right\} \\ \times \sin \frac{\pi p m_i}{L+1} \sin \frac{\pi p m_j}{L+1} \sin \frac{\pi q n_i}{L+1} \sin \frac{\pi q n_j}{L+1}. \quad (91)$$

In table 4, we evaluate this expression for the two other geometries. The same relation holds in this case as

$C_{ij}(L)$	4	6	8	10	12
$(1,1), (L,1)$	1/3	7/29	169/901	13761/89893	3721985/28793575
$(1,1), (L,3)$	1/(2 × 3)	5/29	138/901	12127/89893	3407775/28793575
$(1,1), (L,5)$.	5/(2 × 29)	95/901	9475/89893	2864755/28793575
$(1,1), (L,7)$.	.	95/(2 × 901)	6389/89893	2194565/28793575
$(1,1), (L,9)$.	.	.	6389/(2 × 89893)	1471805/28793575
$(1,1), (L,11)$	1471805/(2 × 28793575)
$C_{ij}(L)$	4	6	8	10	12
$(1,1), (L,1)$	1/3	7/29	169/901	13761/89893	3721985/28793575
$(1,2), (L,2)$	1/6	2/29	30/901	1634/89893	314210/28793575
$(1,3), (L,3)$	1/6	9/29	125/901	11109/89893	3178965/28793575
$(1,4), (L,4)$	1/3	9/29	155/901	4720/89893	984400/28793575
$g_{L/2}$	3	29	901	89893	28793575

Table 4: Top: Correlation function C_{ij} between a monomer at position ($m_i = n_i = 1$) and another at position ($m_j = L, n_j$) for several system sizes L and for $n_j = 1, 3, 5, 7, 9, 11$ (cf. Fig. 20(b)). We notice that the expression of the last line in each row is the half of the expression of the penultimate line. Bottom: Correlation function C_{ij} between opposite side monomers for several system sizes L and for $n_i = n_j = 1, 2, 3, 4$ (see Fig. 20(c)).

well, and we conjecture that the expression of the 2-point correlation takes the following form

$$C_{ij}(L) = \alpha_{ij}^{(2)}(L) g_{L/2}^{-1}, \quad (92)$$

no matter the positions of the two monomers on the boundaries, where $\alpha_{ij}^{(2)}$ depends only of the positions of the two monomers and of the system size L . Consequently, the partition function of the dimer model with two boundary monomers reads

$$Q_2(L) = \alpha_{ij}^{(2)}(L) \cdot g_{L/2} \quad (93)$$

5.3. Partition function with $2n$ boundary monomers

It is worth looking at higher number of monomers to conjecture a more general form of the partition function. We have conjectured that the matrix elements of the correlation matrix are proportional to the sequence $g_{L/2}$, thus thanks to the general pfaffian solution with $2n$ monomers Eq. (86), we obtain the formulas

$$\begin{aligned} Q_2 &= Q_0 \cdot C_{ij}, \\ Q_4 &= Q_0 \cdot (C_{ij}C_{kl} - C_{ik}C_{jl} + C_{il}C_{jk}), \\ Q_6 &= Q_0 \cdot (C_{ij}C_{kl}C_{mn} - C_{il}C_{jk}C_{mn} + C_{il}C_{jm}C_{kn} - \dots), \\ &\vdots \end{aligned} \tag{94}$$

where the pure partition function takes the form Eq. (84), therefore the partition functions are proportional to power of $g_{L/2}$

$$\begin{aligned} Q_0(L) &= 2^{L/2} \cdot g_{L/2}^2, \\ Q_2(L) &= \alpha_{ij}^{(2)}(L) \cdot g_{L/2}, \\ Q_4(L) &= \alpha_{ijkl}^{(4)}(L) \cdot g_{L/2}^0, \\ Q_6(L) &= \alpha_{ijklmn}^{(6)}(L) \cdot g_{L/2}^{-1}, \\ &\vdots \end{aligned} \tag{95}$$

which can be generalized for $2n$ monomers at positions i_1, i_2, \dots, i_{2n}

$$Q_{2n}(L) = \alpha_{i_1 i_2 \dots i_{2n}}^{(2n)}(L) \cdot g_{L/2}^{2-n}, \tag{96}$$

in such way that a relation between Q_{2p} et Q_{2q} can be founded ($p, q \geq 1$), dropping all the indices but p and q for simplicity, we found *ex hypothesi*

$$\boxed{\frac{Q_{2p}}{Q_{2q}} = \frac{\alpha^{(2p)}}{\alpha^{(2q)}} g^{q-p}}, \tag{97}$$

valid for $2p$ and $2q$ monomers anywhere on the boundaries of the square lattice. Finally all these numerical relations between dimer partition functions with and without boundary monomers are the consequence of Eq. (86) and Eq. (92), which are unfortunately no longer valid for bulk monomers.

6. Conclusion

In this work the classical dimer model was discussed in great details both in a fermionic and bosonic field theory formulation. The bosonic formulation of the dimer model is based on the so-called height mapping and it is well suited for phenomenological predictions about correlations between dimers and monomers in a Coulomb gas context. Then we presented a practical and complete fermionic solution of the $2d$ dimer model on the square lattice with an arbitrary number of monomers. Furthermore, the Tzeng-Wu solution of the dimer model with a boundary monomer was found to be included in our theory. Interpretations of finite size effects of the Tzeng-Wu solution in a CFT/Coulomb gas framework has been performed, and we showed that a careful examination of boundary conditions in the model allowed us to recover the central charge of the free fermion/free boson field theory. The exact expression of correlation functions between monomers has been written in terms of the product of two pfaffians, and we gave an explicit formula for boundary correlations

valid for the four boundaries of the rectangle. This solution has been used to compute correlations for several configurations in order to extract bulk, surface and corner scaling dimensions for dimer and monomer operators. All these results were interpreted in the Coulomb gas formalism, and we showed that all the predictions of the CFT were in accordance with a $c = 1$ theory. Last but not least, the exact closed-form expression of correlations between boundary monomers has been extensively used to extract some combinatorial and numerical informations about the partition function of the model. Furthermore, an unexpected relation has been found between partition functions with and without boundary monomers, and has been demonstrated thanks to our pfaffian solution. Generally, this Grassmann method can also be used for studying more general correlation functions, thermodynamical quantities, or transport phenomena of monomers. Other types of lattices, such as hexagonal lattice and other boundary conditions, can also be considered, as well as more precise comparisons with CFT results about rectangle geometry [130]. The same analysis of corner contribution to free energy as well as critical exponents can be studied in the interacting dimer model using the height mapping and results will be presented elsewhere. A future challenge emerging out of this present work is the study of other two dimensional dimer related models as the trimer model [53] or the four-color model [92, 46] which can be seen as an interacting colored dimer model. Work in those directions is in progress.

Appendices

A. Grassmann variables, determinant permanent and all that

A n -dimensional Grassmann algebra ²¹ is the algebra generated by a set of variables $\{a_i\}$, with $i = 1..n$ satisfying

$$\{a_i, a_j\} = 0, \quad (98)$$

i.e. they anti-commute, which implies in particular that $a_i^2 = 0$. The algebra generated by these quantities contains all expressions of the form

$$\begin{aligned} f(a) &= f^{(0)} + \sum_i f^i a_i + \sum_{i < j} f^{ij} a_i a_j + .. \\ &= \sum_{0 \leq p \leq n} \sum_i \frac{1}{p!} f^{i_1 \dots i_p} a_{i_1} a_{i_2} \dots a_{i_p}, \end{aligned} \quad (99)$$

where the coefficients are antisymmetric tensors with p indices, each ranging from 1 to n . Since there are $\binom{n}{p}$ such linearly independent tensors, summing over p from 0 to n produces a 2^n -dimensional algebra. The anticommuting rule allows us to define an associative product

$$f_1(a) f_2(a) = f_1^0 f_2^0 + \sum_i (f_1^0 f_2^i + f_1^i f_2^0) a_i + \frac{1}{2} \sum_{ij} (f_1^{ij} f_2^0 + f_1^i f_2^j - f_1^j f_2^i + f_1^0 f_2^{ij}) a_i a_j + .. \quad (100)$$

Please note that in general fg is not equal to $\pm gf$. Nevertheless the subalgebra containing terms with an even number (possibly zero) of a variables commutes with any element f . Having defined sum and products in the Grassmann algebra we now define a left derivative $\partial_i := \partial_{a_i}$. The derivative gives zero on a monomial which does not contain the variable a_i . If the monomial does contain a_i , it is moved to the left (with the appropriate sign due to the exchanges) and then suppressed. The operation is extended by linearity to any element of the algebra. A right derivative can be defined similarly. From this definition the following rules can be obtained

$$\begin{aligned} \{\partial_i, \partial_j\} &= 0 \\ \{\partial_i, a_j\} &= \delta_{ij}. \end{aligned} \quad (101)$$

Integrals are defined as linear operations over the functions f with the property that they can be identified with the (left) derivatives [12]. Correspondingly

$$\begin{aligned} \int da_i f(a) &= \partial_i f(a), \\ \int da_i da_j f(a) &= \partial_i \partial_j f(a), \end{aligned} \quad (102)$$

which leads to the generalization

$$\int da_{i_k} da_{i_{k-1}} \dots da_{i_1} f(a) = \partial_{i_k} \partial_{i_{k-1}} \dots \partial_{i_1} f. \quad (103)$$

²¹The presentation closely follows [66].

It is obvious that this definition fulfills the constraint of translational invariance

$$\int dc(c_1 + c_2 a) = \int dc[c_1 + c_2(a + b)], \quad (104)$$

which requires

$$\int da_i a_j = \delta_{ij}. \quad (105)$$

Changes of coordinates are required to preserve the anti-commuting structure of the Grassmann algebra, this allows non-singular linear transformations of the form $b_i = \sum_j A_{ij} a_j$. One then can verify that by setting $f(a) = F(b)$ one can obtain the following relation

$$\int \prod_i da_i f(a) = \det A \int \prod_i db_i F(b), \quad (106)$$

at variance with the commuting case in which the factor on the right hand side would have been $\det^{-1} A$. We define $\int \mathcal{D}[a, \bar{a}] = \int \prod_i da_i d\bar{a}_i$ the Grassmann measure. In the multidimensional integral, the symbols da_1, \dots, da_N are again anticommuting with each other. The basic expression of the Grassmann analysis concern the Gaussian fermionic integrals [128] which is related to the determinant

$$\det A = \int \mathcal{D}[a, \bar{a}] \exp \left(\sum_{i,j=1}^N a_i A_{ij} \bar{a}_j \right), \quad (107)$$

where $\{a_i, \bar{a}_i\}$ is a set of completely anticommuting Grassmann variables, the matrix in the exponential is arbitrary. The two Grassmann variables a_i and \bar{a}_i are independent and not conjugate to each other, they can be seen as composante of a complex Grassmann variables. The Gaussian integral of the second kind is related to the Pfaffian of the associated skew-symmetric matrix

$$\text{pf} A = \int \mathcal{D}[a] \exp \left(\frac{1}{2} \sum_{i,j=1}^N a_i A_{ij} a_j \right). \quad (108)$$

The pfaffian form is a combinatorial polynomial in A_{ij} , known in mathematics for a long time. The pfaffian and determinant of the associated skew-symmetric matrix are algebraically related by $\det A = (\text{pf} A)^2$. This relation can be most easily proved in terms of the fermionic integrals. The linear superpositions of Grassmann variables are still Grassmann variables and it is possible to make a linear change of variables in the integrals. The only difference with the rules of the common analysis, is that the Jacobian will now appear in the inverse power. New variables of integration can be introduced, in particular, by means of the transformation to the momentum space. The permanent of A and the so-called hafnian can be written with Grassmann variables as well

$$\begin{aligned} \text{perm} A &= \int \mathcal{D}[b, \bar{b}] \int \mathcal{D}[a, \bar{a}] \exp \left(\sum_{i,j=1}^N a_i \bar{a}_i A_{ij} b_j \bar{b}_j \right), \\ \text{hf} A &= \int \mathcal{D}[a, \bar{a}] \exp \left(\frac{1}{2} \sum_{i,j=1}^N a_i \bar{a}_i A_{ij} a_j \bar{a}_j \right), \end{aligned} \quad (109)$$

which are connected by the formula $\text{perm}A = (\text{hf}A)^2$. We recall that the definition of the permanent differs from that of the determinant in that the signatures of the permutations are not taken into account.

B. Plechko mirror symmetry

In this appendix we briefly recall the method of resolution of the $2d$ dimer model based on the integration over Grassmann variables and factorization principles for the partition function introduced in the context of $2d$ Ising model [118]. The general partition function for a graph with N vertices

$$Q_0 = \int \mathcal{D}[\eta] \exp\left(\frac{1}{2} \sum_{i,j=1}^N \eta_i A_{ij} \eta_j\right), \quad (110)$$

can be written, for a square lattice of size $L \times L$ with L even, as

$$Q_0 = \int \mathcal{D}[\eta] \prod_{m,n}^L (1 + t_x \eta_{mn} \eta_{m+1n}) (1 + t_y \eta_{mn} \eta_{mn+1}), \quad (111)$$

where η_{mn} are nilpotent and commuting variables on every vertices of the square lattice. The integrals can be done if we introduce a set of Grassmann variables $(a_{mn}, \bar{a}_{mn}, b_{mn}, \bar{b}_{mn})$, (cf. Fig. 21(a)), such that

$$\begin{aligned} (1 + t_x \eta_{mn} \eta_{m+1n}) &= \int \mathcal{D}[\bar{a}] \mathcal{D}[a] e^{a_{mn} \bar{a}_{mn}} (1 + a_{mn} \eta_{mn}) (1 + t_x \bar{a}_{mn} \eta_{m+1n}), \\ (1 + t_y \eta_{mn} \eta_{mn+1}) &= \int \mathcal{D}[\bar{b}] \mathcal{D}[b] e^{b_{mn} \bar{b}_{mn}} (1 + b_{mn} \eta_{mn}) (1 + t_y \bar{b}_{mn} \eta_{mn+1}). \end{aligned} \quad (112)$$

This decomposition allows for an integration over variables η_{mn} , after rearranging the different link variables $A_{mn} := 1 + a_{mn} \eta_{mn}$, $\bar{A}_{m+1n} := 1 + t_x \bar{a}_{mn} \eta_{m+1n}$, $B_{mn} := 1 + b_{mn} \eta_{mn}$ and $\bar{B}_{mn+1} := 1 + t_y \bar{b}_{mn} \eta_{mn+1}$. Then the partition function becomes

$$Q_0 = \text{Tr}_{\{a, \bar{a}, b, \bar{b}, \eta\}} \prod_{m,n}^L (A_{mn} \bar{A}_{m+1n}) (B_{mn} \bar{B}_{mn+1}), \quad (113)$$

where we use the notation for the measure of integration

$$\text{Tr}_{\{a, \bar{a}, b, \bar{b}, \eta\}} X(a, \bar{a}, b, \bar{b}, \eta) = \int \mathcal{D}[\bar{a}] \mathcal{D}[a] \mathcal{D}[\bar{b}] \mathcal{D}[b] \mathcal{D}[\eta] \prod_{mn} e^{a_{mn} \bar{a}_{mn} + b_{mn} \bar{b}_{mn}} X(a, \bar{a}, b, \bar{b}, \eta). \quad (114)$$

Then, the non-commuting link variables are moved in such a way that each η_{mn} is isolated and can be integrated directly. This rearrangement is possible in two dimensions thanks to the mirror ordering introduced by Plechko

for the Ising model. The ordering process can be detailed as follow

$$\begin{aligned}
\prod_{m,n}^L (A_{mn} \bar{A}_{m+1n}) (B_{mn} \bar{B}_{mn+1}) &= \prod_{n=1}^{\overrightarrow{L}} (A_{1n} \bar{A}_{2n}) (B_{1n} \bar{B}_{1n+1}) (A_{2n} \bar{A}_{3n}) (B_{2n} \bar{B}_{2n+1}) \cdots \\
&= \prod_{n=1}^{\overrightarrow{L}} (A_{1n} \bar{A}_{2n}) (A_{2n} \bar{A}_{3n}) \cdots (B_{1n} B_{2n} \cdots \bar{B}_{2n+1} \bar{B}_{1n+1}) \\
&= \prod_{n=1}^{\overrightarrow{L}} (B_{1n} (A_{1n} \bar{A}_{2n}) B_{2n} (A_{2n} \bar{A}_{3n}) \cdots \bar{B}_{2n+1} \bar{B}_{1n+1}) \\
&= \prod_{n=1}^{\overrightarrow{L}} (\bar{B}_{Ln} \cdots \bar{B}_{2n} \bar{B}_{1n}) (B_{1n} A_{1n} \bar{A}_{2n} B_{2n} A_{2n} \bar{A}_{3n} \cdots \bar{A}_{Ln} B_{Ln} A_{Ln}), \quad (115)
\end{aligned}$$

where the products are ordered according to the orientation of the arrows. The Grassmann terms in brackets (\cdots) on the first line of the previous equation are commuting objects, since they are integral representations of commuting scalars. This also imposes the boundary conditions $\bar{A}_{1n} = 1$, $\bar{A}_{L+1n} = 1$, $\bar{B}_{m1} = 1$, and $\bar{B}_{mL+1} = 1$, or $\bar{a}_{0n} = \bar{a}_{Ln} = \bar{b}_{m0} = \bar{b}_{mL} = 0$ (for open boundary conditions only). We finally obtain the following exact expression

$$Q_0 = \text{Tr}_{\{a, \bar{a}, b, \bar{b}, \eta\}} \prod_{n=1}^{\overrightarrow{L}} \left(\prod_{m=1}^{\overleftarrow{L}} \bar{B}_{mn} \prod_{m=1}^{\overrightarrow{L}} \bar{A}_{mn} B_{mn} A_{mn} \right). \quad (116)$$

The integration over the η_{mn} variables is performed exactly, recursively from $m = 1$ to $m = L$ for each n . Each integration leads to a quantity $L_{mn} = a_{mn} + b_{mn} + t_x \bar{a}_{m-1n} + (-1)^{m+1} t_y \bar{b}_{mn-1}$ which is moved to the left of the products over m , hence a minus sign is needed in front of \bar{b} each time a L_{mn} crosses the product of \bar{B} terms on the left. Finally

$$Q_0 = \text{Tr}_{\{a, \bar{a}, b, \bar{b}\}} \prod_{m,n}^{\overrightarrow{L}} L_{mn}, \quad (117)$$

becomes an integration over products of linear Grassmann terms. This can be further simplified by introducing additional Grassmann variables c_{mn} such that

$$L_{mn} = \int dc_{mn} \exp(c_{mn} L_{mn}). \quad (118)$$

This expresses Q_0 as a Gaussian integral over variables $(a, \bar{a}, b, \bar{b}, c)$, and therefore Q_0 is a simple determinant of a quadratic form. Indeed, after partially integrating over variables (a, \bar{a}, b, \bar{b}) and symmetrization of the expressions, one obtains

$$\begin{aligned}
Q_0 &= \text{Tr}_{\{a, \bar{a}, b, \bar{b}, c\}} \exp \left(\sum_{mn} c_{mn} L_{mn} \right) \\
&= \int \mathcal{D}[c] \exp \sum_{mn} \left[\frac{1}{2} t_x (c_{m+1n} c_{mn} - c_{m-1n} c_{mn}) + \frac{1}{2} t_y (-1)^{m+1} (c_{mn+1} c_{mn} - c_{mn-1} c_{mn}) \right] \\
&= \int \mathcal{D}[c] \exp S_0. \quad (119)
\end{aligned}$$

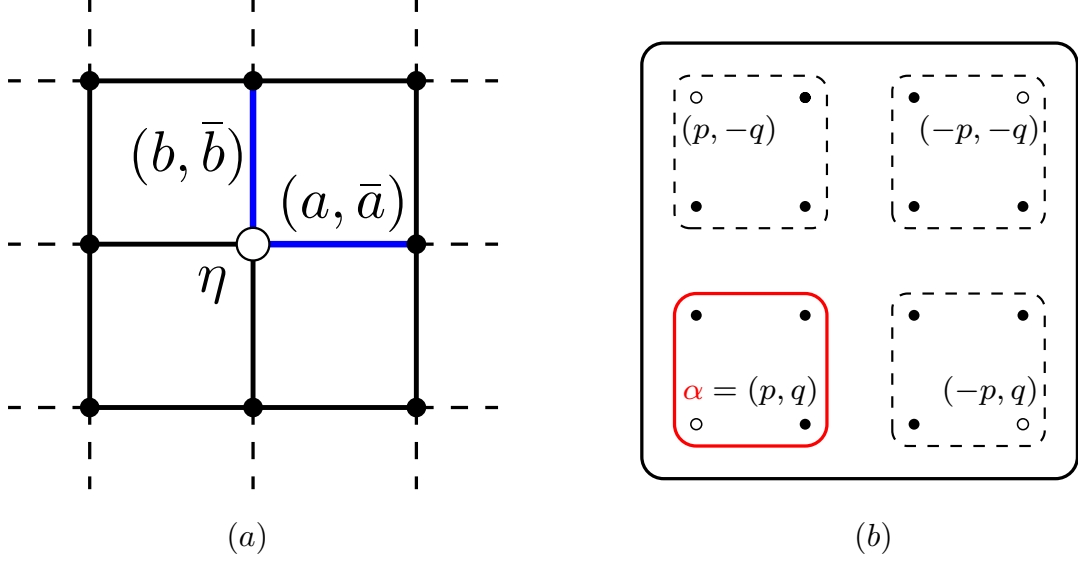


Figure 21: (a) Grassmann representation for each dimer, with one nilpotent variable η per site, and two pairs of Grassmann variables for the two directions along the links connecting two neighboring sites. (b) Block partition of the Fourier modes. The modes considered in the summation Eq. (123) belongs to the sector inside the reduce domain (red delimitation) $1 \leq p, q \leq L/2$. For one point labeled $\alpha = (p, q)$ inside this domain correspond 3 others points related by symmetry $p \rightarrow L+1-p$ and $q \rightarrow L+1-q$ (open circles).

The computation of the determinant of this quadratic form can be done simply using Fourier transform satisfying open boundary conditions

$$c_{mn} = \frac{2i^{m+n}}{L+1} \sum_{p,q=1}^L c_{pq} \sin\left(\frac{\pi pm}{L+1}\right) \sin\left(\frac{\pi qn}{L+1}\right), \quad (120)$$

with $c_{0n} = c_{L+1n} = c_{m0} = c_{mL+1} = 0$. Inserting Eq. (120) into Eq. (119), and using two following sum identities

$$\frac{2}{L+1} \sum_{m=1}^L \sin\left(\frac{\pi pm}{L+1}\right) \sin\left(\frac{\pi qm}{L+1}\right) = \delta_{p,q}, \quad (121)$$

$$\frac{2}{L+1} \sum_{m=1}^L (-1)^{m+1} \sin\left(\frac{\pi pm}{L+1}\right) \sin\left(\frac{\pi qm}{L+1}\right) = \delta_{p+q, L+1}, \quad (122)$$

we can finally put Eq. (119) into a block form of 4 independent Grassmann variables

$$S_0 = \sum_{p,q}^{L/2} 2it_x \cos \frac{\pi p}{L+1} (c_{pq}c_{-p-q} + c_{p-q}c_{-pq}) + 2it_y \cos \frac{\pi q}{L+1} (c_{pq}c_{p-q} + c_{-pq}c_{-p-q}), \quad (123)$$

where, for example, c_{-pq} is a short notation for c_{L+1-pq} . The summation is performed only for 1/4 of the Fourier modes, (see Fig. 21(b)), since the other are related by the symmetry $p \rightarrow L+1-p$ and $q \rightarrow L+1-q$. This block representation is convenient for computing the remaining integrals over the momenta, as a product

of cosine functions as found by Kasteleyn Temperley and Fischer

$$Q_0 = \prod_{p,q=1}^{L/2} \left[4t_x^2 \cos^2 \frac{\pi p}{L+1} + 4t_y^2 \cos^2 \frac{\pi q}{L+1} \right]. \quad (124)$$

The main ingredient of this recipe is the mirror factorization Eq. (116) of the partition function, which allows a direct integration over nilpotent variables. This mirror factorization is then the major obstacle to the generalization of this formalism in $d > 2$. Indeed, for the $3d$ case, a generalization of this factorization is far from obvious and remains to find.

C. General monomer-dimer partition function

The general monomer-dimer problem is a much more complex and challenging problem in statistical physics and combinatorics, because the position of the monomers are not fixed either than their number (*cf.* Fig. 22 for $L = 2$). From the point of view of theoretical physics, the number of monomers divided by the number of occupied site defines the monomer density ρ . It is long known that the full phase diagram of the monomer-dimer model does not admit any phase transition for $\rho > 0$ [59, 60]. Furthermore the behavior of monomer-monomer correlations for finite density has been studied numerically [102], and strong evidences for exponential correlations has been established, in accordance with mean-field calculations using Grassmann variables [115]. From a computational point of view, the problem has been shown to belong to the $\#P$ -complete enumeration class [76] and all the methods available are either efficient but approximative [8, 83] or exact but desperately slow [1]. In this short appendix one shows how to use our exact solution to express the partition function of this enumerative problem. Let us start by counting the number of ways $N_{2p}(M, N)$ of choosing the positions

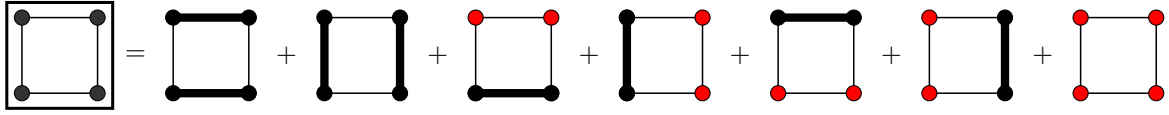


Figure 22: Number of configurations of the general monomer-dimer model for a 2×2 square lattice.

of $2p$ monomers on a $M \times N$ lattice, the result is a simple binomial expression $N_{2p}(M, N) = \binom{M^2/2}{p} \binom{N^2/2}{p}$. Using this formula we can sum up over the number of monomers $2p$ to obtain the number of ways to choose the positions of the monomers. Finally the number of terms in the full partition function is one (the pure dimer model) plus all the terms with an even number of monomers (one choose $M = N = L$ for simplicity)

$$N(L) = 1 + \sum_{p=1}^{L^2/2} N_{2p}(L) = \frac{2^{L^2/2} \Gamma(\frac{L^2+1}{2})}{\sqrt{\pi} \Gamma(\frac{L^2+2}{2})}. \quad (125)$$

This number grows as 2^{L^2} when the size of the lattice goes to infinity, making the problem impossible to solve analytically. Since our method allows to calculate exactly the partition function of the the dimer model on a square lattice of size $M \times N$ with an arbitrary even number of monomers, then we can formally write down the full monomer-dimer partition function as a sum over the number and the positions of monomers

$$\mathcal{Z} = Q_0 + \sum_{\{r_i\}} Q_2 + \sum_{\{r_i\}} Q_4 + \dots \quad (126)$$

which becomes simpler in the boundary case

$$\mathcal{Z} = Q_0 \left[1 + \sum_{ij} C_{ij} + \sum_{ijkl} (C_{ij} C_{kl} \pm \text{permutation}) + \sum_{ijklmn} (C_{ij} C_{kl} C_{mn} \pm \text{permutation}) + \dots \right]. \quad (127)$$

The general formula Eq. (126) allows for the numerical computation of the full partition function for small system sizes up to $L = 8$. Unfortunately, our method belong to the second category, the algorithm time grows exponentially with the size of the system.

$M \backslash N$	2	4	6	8
2	7	71	733	7573
4	71	10012	1453535	211351945
6	733	1453535	2989126727	61582117253688
8	7573	211351945	6158217253688	179788343101980135

Table 5: Number of configurations of the general monomer-dimer model for a $L \times L$ square lattice computed using Eq. (126).

References

- [1] J. H. Ahrens. Paving the chessboard. *Journal of Combinatorial Theory, Series A*, 31(3):277–288, 1981.
- [2] D. Alberici and P. Contucci. Solution of the Monomer-Dimer Model on Locally Tree-Like Graphs. Rigorous Results. *Communications in Mathematical Physics*, pages 1–29, 2013.
- [3] F. Alet, Y. Ikhlef, J. L. Jacobsen, G. Misguich, and V. Pasquier. Classical dimers with aligning interactions on the square lattice. *Physical Review E*, 74(4):041124, 2006.
- [4] F. Alet, J. L. Jacobsen, G. Misguich, V. Pasquier, F. Mila, and M. Troyer. Interacting classical dimers on the square lattice. *Physical Review Letters*, 94(23):235702, 2005.
- [5] N. Allegra and J.-Y. Fortin. Grassmannian representation of the two-dimensional monomer-dimer model. *Physical Review E*, 89(6):062107, 2014.
- [6] H. Au-Yang and J. H. H. Perk. Ising correlations at the critical temperature. *Physics Letters A*, 104(3):131–134, 1984.
- [7] A. Ayyer. A statistical model of current loops and magnetic monopoles. *arXiv preprint arXiv:1311.5965*, 2013.
- [8] R. J. Baxter. Dimers on a rectangular lattice. *Journal of Mathematical Physics*, 9(4):650–654, 1968.
- [9] R. J. Baxter. Partition function of the eight-vertex lattice model. *Ann. Phys.*, 70(1):193–228, 1972.
- [10] R. J. Baxter. *Exactly solved models in statistical mechanics*. Courier Dover Publications, 2007.
- [11] A. A. Belavin, A. M. Polyakov, and A. B. Zamolodchikov. Infinite conformal symmetry in two-dimensional quantum field theory. *Nuclear Physics B*, 241(2):333–380, 1984.
- [12] F. A. Berezin. *The Method of second quantization*. Academic Press, 1966.
- [13] H. Bethe. Zur Theorie der Metalle. *Zeitschrift für Physik*, 71(3-4):205–226, 1931.
- [14] S. M. Bhattacharjee, J. F. Nagle, D. A. Huse, and M. E. Fisher. Critical behavior of a three-dimensional dimer model. *Journal of Statistical Physics*, 32(2):361–374, 1983.
- [15] H. Blöte, J. L. Cardy, and M. Nightingale. Conformal invariance, the central charge, and universal finite-size amplitudes at criticality. *Physical Review Letters*, 56(7):742, 1986.
- [16] H. Blöte and H. Hilborst. Roughening transitions and the zero-temperature triangular ising antiferromagnet. *Journal of Physics A: Mathematical and General*, 15(11):L631, 1982.
- [17] R. Bondesan, J. Dubail, J. L. Jacobsen, and H. Saleur. Conformal boundary state for the rectangular geometry. *Nuclear Physics B*, 862(2):553–575, 2012.
- [18] R. Bondesan, J. L. Jacobsen, and H. Saleur. Rectangular amplitudes, conformal blocks, and applications to loop models. *Nuclear Physics B*, 867(3):913–949, 2013.
- [19] J. Bouttier, M. Bowick, E. Guitter, and M. Jeng. Vacancy localization in the square dimer model. *Physical Review E*, 76:041140, Oct 2007.
- [20] J. Brankov. Isomorphism of dimer configurations and spanning trees on finite square lattices. *Journal of Mathematical Physics*, 36(9):5071–5083, 1995.

- [21] S. Caracciolo, J. L. Jacobsen, H. Saleur, A. D. Sokal, and A. Sportiello. Fermionic field theory for trees and forests. *Physical Review Letters*, 93(8):080601, 2004.
- [22] S. Caracciolo, A. D. Sokal, and A. Sportiello. Grassmann integral representation for spanning hyperforests. *Journal of Physics A: Mathematical and Theoretical*, 40(46):13799, 2007.
- [23] J. L. Cardy. Effect of boundary conditions on the operator content of two-dimensional conformally invariant theories. *Nuclear Physics B*, 275(2):200–218, 1986.
- [24] J. L. Cardy. Boundary conditions, fusion rules and the Verlinde formula. *Nuclear Physics B*, 324(3):581–596, 1989.
- [25] J. L. Cardy and I. Peschel. Finite-size dependence of the free energy in two-dimensional critical systems. *Nuclear Physics B*, 300:377–392, 1988.
- [26] M. Ciucu. Dimer packings with gaps and electrostatics. *Proc. Nat. Acad. Sci.*, 105(8):2766–2772, 2008.
- [27] M. Ciucu. The emergence of the electrostatic field as a Feynman sum in random tilings with holes. *Transactions of the American Mathematical Society*, 362(9):4921–4954, 2010.
- [28] M. Clusel and J.-Y. Fortin. Boundary field induced first-order transition in the 2D Ising model: exact study. *J. Phys. A: Mathematical and General*, 39(5):995, 2006.
- [29] M. Clusel and J.-Y. Fortin. Grassmann techniques applied to classical spin systems. *Condensed Matter Physics*, 12(3):463, 2009.
- [30] M. Clusel, J.-Y. Fortin, and V. N. Plechko. Alternative description of the 2D Blume-Capel model using Grassmann algebra. *Journal of Physics A: Mathematical and Theoretical*, 41(40):405004, 2008.
- [31] H. Cohn, N. Elkies, J. Propp, et al. Local statistics for random domino tilings of the Aztec diamond. *Duke Mathematical Journal*, 85(1):117–166, 1996.
- [32] R. Costa-Santos and B. M. McCoy. Dimers and the critical Ising model on lattices of genus > 1 . *Nuclear Physics B*, 623(3):439–473, 2002.
- [33] K. Damle, D. Dhar, and K. Ramola. Resonating valence bond wave functions and classical interacting dimer models. *Physical review letters*, 108(24):247216, 2012.
- [34] D. Dhar and S. Chandra. Exact entropy of dimer coverings for a class of lattices in three or more dimensions. *Physical review letters*, 100(12):120602, 2008.
- [35] P. Di Francesco, D. Sénéchal, and P. Mathieu. *Conformal field theory*. Springer, 1997.
- [36] J. Dubédat. Dimers and analytic torsion I. *arXiv preprint arXiv:1110.2808*, 2011.
- [37] N. Elkies, G. Kuperberg, M. Larsen, and J. Propp. Alternating-sign matrices and domino tilings (Part I). *Journal of Algebraic Combinatorics*, 1(2):111–132, 1992.
- [38] V. Elser. Solution of the dimer problem on a hexagonal lattice with boundary. *Journal of Physics A: Mathematical and General*, 17(7):1509, 1984.
- [39] P. Fendley, R. Moessner, and S. L. Sondhi. Classical dimers on the triangular lattice. *Physical Review B*, 66(21):214513, 2002.
- [40] A. E. Ferdinand. Statistical mechanics of dimers on a quadratic lattice. *Journal of Mathematical Physics*, 8(12):2332–2339, 1967.

- [41] M. E. Fisher. Statistical mechanics of dimers on a plane lattice. *Physical. Review*, 124(6):1664, 1961.
- [42] M. E. Fisher and R. E. Hartwig. Toeplitz determinants: some applications, theorems, and conjectures. In K. E. Shuler, editor, *Stochastic Processes in Chemical Physics*, volume 15, page 333. John Wiley & Sons, 1969.
- [43] M. E. Fisher and J. Stephenson. Statistical mechanics of dimers on a plane lattice. II. Dimer correlations and monomers. *Physical Review*, 132(4):1411, 1963.
- [44] J. Fjærestad. Classical and quantum dimers on the star lattice. *Bulletin of the American Physical Society*, 54, 2009.
- [45] J. Fjærestad. The 3-edge-colouring problem on the 4–8 and 3–12 lattices. *Journal of Statistical Mechanics: Theory and Experiment*, 2010(01):P01004, 2010.
- [46] J. Fjærestad. Dimer and fermionic formulations of a class of colouring problems. *Journal of Physics A: Mathematical and Theoretical*, 45(7):075001, 2012.
- [47] P. Flajolet and R. Sedgewick. *Analytic combinatorics*. Cambridge University Press, 2009.
- [48] J.-Y. Fortin and M. Clusel. Second-order critical lines of spin-S Ising models in a splitting field using Grassmann techniques. *Physical Review B*, 78(17):172402, 2008.
- [49] R. H. Fowler and G. S. Rushbrooke. An attempt to extend the statistical theory of perfect solutions. *Trans. Faraday Soc.*, 33:1272–1294, 1937.
- [50] E. Fradkin. *Field theories of condensed matter physics*. Cambridge University Press, 2013.
- [51] E. Fradkin and L. P. Kadanoff. Disorder variables and para-fermions in two-dimensional statistical mechanics. *Nuclear Physics B*, 170(1):1–15, 1980.
- [52] S. Franco, A. Hanany, D. Vegh, B. Wecht, and K. D. Kennaway. Brane dimers and quiver gauge theories. *Journal of High Energy Physics*, 2006(01):096, 2006.
- [53] A. Ghosh, D. Dhar, and J. L. Jacobsen. Random trimer tilings. *Physical Review E*, 75(1):011115, 2007.
- [54] A. Hanany and K. D. Kennaway. Dimer models and toric diagrams. *arXiv preprint hep-th/0503149*, 2005.
- [55] R. E. Hartwig. Monomer pair correlations. *Journal of Mathematical Physics*, 7:286–299, 1966.
- [56] R. Hayn and V. N. Plechko. Free fermion solution for dimer problem. *JINR Rapid Communications*, 61(4):18, 1993.
- [57] R. Hayn and V. N. Plechko. Grassmann variable analysis for dimer problems in two dimensions. *Journal of Physics A*, 27:4753, 1994. cond-mat/9711156.
- [58] O. J. Heilmann and E. H. Lieb. Monomers and dimers. *Physical Review Letters*, 24:1412–1414, 1970.
- [59] O. J. Heilmann and E. H. Lieb. Theory of monomer-dimer systems. *Communication in Mathematical Physics*, 25(3):190–232, 1972. reprinted in: *Statistical Mechanics*, edited by B. Nachtergaele, J. P. Solovej, and J. Yngvason, Springer (2004), pp. 45–87.
- [60] O. J. Heilmann and E. H. Lieb. Theory of monomer-dimer systems. In *Statistical Mechanics*, pages 45–87. Springer, 2004.
- [61] M. Henkel. *Conformal invariance and critical phenomena*. Springer, 1999.

- [62] C. L. Henley. Relaxation time for a dimer covering with height representation. *Journal of Statistical Physics*, 89(3-4):483–507, 1997.
- [63] D. A. Huse, W. Krauth, R. Moessner, and S. Sondhi. Coulomb and liquid dimer models in three dimensions. *Physical Review Letters*, 91(16):167004, 2003.
- [64] F. Iglói, I. Peschel, and L. Turban. Inhomogeneous systems with unusual critical behaviour. *Advances in Physics*, 42(6):683–740, 1993.
- [65] L. Ioffe and A. Larkin. Superconductivity in the liquid-dimer valence-bond state. *Physical Review B*, 40(10):6941, 1989.
- [66] C. Itzykson and J.-M. Drouffe. *Statistical Field Theory: Volume 1, From brownian motion to renormalization and lattice gauge theory*. Cambridge University Press, 1991.
- [67] C. Itzykson, H. Saleur, and J.-B. Zuber. Conformal invariance of nonunitary 2d-models. *EPL (Europhysics Letters)*, 2(2):91, 1986.
- [68] N. S. Izmailian and R. Kenna. Dimer model on a triangular lattice. *Physical Review E*, 84(2):021107, 2011.
- [69] N. S. Izmailian, R. Kenna, W. Guo, and X. Wu. Exact finite-size corrections and corner free energies for the $c = -2$ universality class. *Nuclear Physics B*, 884:157–171, 2014.
- [70] N. S. Izmailian, K. Oganesyan, and C.-K. Hu. Exact finite-size corrections of the free energy for the square lattice dimer model under different boundary conditions. *Physical Review E*, 67(6):066114, 2003.
- [71] N. S. Izmailian, K. Oganesyan, M.-C. Wu, and C.-K. Hu. Finite-size corrections and scaling for the triangular lattice dimer model with periodic boundary conditions. *Physical Review E*, 73(1):016128, 2006.
- [72] N. S. Izmailian, V. B. Priezzhev, P. Ruelle, and C.-K. Hu. Logarithmic conformal field theory and boundary effects in the dimer model. *Physical Review Letters*, 95:260602, Dec 2005.
- [73] J. L. Jacobsen. Bulk, surface and corner free-energy series for the chromatic polynomial on the square and triangular lattices. *Journal of Physics A: Mathematical and Theoretical*, 43(31):315002, 2010.
- [74] J. L. Jacobsen and J. Kondev. Field theory of compact polymers on the square lattice. *Nuclear Physics B*, 532(3):635–688, 1998.
- [75] M. Jeng, M. J. Bowick, W. Krauth, J. Schwarz, and X. Xing. Vacancy diffusion in the triangular-lattice dimer model. *Physical Review E*, 78(2):021112, 2008.
- [76] M. R. Jerrum. Two-dimensional monomer-dimer systems are computationally intractable. *Journal of Statistical Physics*, 48(1-2):121–134, 1987. Erratum-ibid **59**, 1087-1088 (1990).
- [77] P. E. John and H. Sachs. On a strange observation in the theory of the dimer problem. *Discrete Mathematics*, 216(1):211–219, 2000.
- [78] L. P. Kadanoff and H. Ceva. Determination of an operator algebra for the two-dimensional Ising model. *Physical Review B*, 3(11):3918, 1971.
- [79] P. W. Kasteleyn. The statistics of dimers on a lattice: I. the number of dimer arrangements on a quadratic lattice. *Physica*, 27(12):1209–1225, 1961.
- [80] P. W. Kasteleyn. Dimer statistics and phase transitions. *Journal of Mathematical Physics*, 4:287, 1963.

- [81] B. Kaufman. Crystal statistics. II. Partition function evaluated by spinor analysis. *Physical Review*, 76(8):1232, 1949.
- [82] B. Kaufman and L. Onsager. Crystal statistics. III. Short-range order in a binary Ising lattice. *Physical Review*, 76(8):1244, 1949.
- [83] C. Kenyon, D. Randall, and A. Sinclair. Approximating the number of monomer-dimer coverings of a lattice. *Journal of Statistical Physics*, 83(3-4):637–659, 1996.
- [84] R. Kenyon. Local statistics of lattice dimers. In *Annales de l’Institut Henri Poincaré (B) Probability and Statistics*, volume 33, pages 591–618. Elsevier, 1997.
- [85] R. Kenyon. Conformal invariance of domino tiling. *Annals of probability*, pages 759–795, 2000.
- [86] R. Kenyon. Dominos and the gaussian free field. *Annals of probability*, pages 1128–1137, 2001.
- [87] R. Kenyon. Conformal invariance of loops in the double-dimer model. *Communications in Mathematical Physics*, 326(2):477–497, 2014.
- [88] R. W. Kenyon and D. B. Wilson. Double-dimer pairings and skew young diagrams. *Electronic Journal of Combinatorics*, 18(1), 2011.
- [89] P. Kleban and I. Vassileva. Free energy of rectangular domains at criticality. *Journal of Physics A: Mathematical and General*, 24(14):3407, 1991.
- [90] P. Kleban and I. Vassileva. Domain boundary energies in finite regions at $2d$ criticality via conformal field theory. *Journal of Physics A: Mathematical and General*, 25(22):5779, 1992.
- [91] D. Klein and T. Schmalz. Exact enumeration of long-range-ordered dimer coverings on the square-planar lattice. *Physical Review B*, 41(4):2244, 1990.
- [92] J. Kondev and C. L. Henley. Four-coloring model on the square lattice: A critical ground state. *Physical Review B*, 52(9):6628, 1995.
- [93] J. Kondev and J. L. Jacobsen. Conformational entropy of compact polymers. *Physical Review Letters*, 81(14):2922, 1998.
- [94] X. P. Kong. *Wave-Vector Dependent Susceptibility of the Two-Dimensional Ising Model*. PhD thesis, State University of New York at Stony Brook, 1987.
- [95] Y. Kong. Logarithmic corrections in the free energy of monomer-dimer model on plane lattices with free boundaries. *Physical Review E*, 74(1):011102, 2006.
- [96] Y. Kong. Monomer-dimer model in two-dimensional rectangular lattices with fixed dimer density. *Physical Review E*, 74(6):061102, 2006.
- [97] Y. Kong. Packing dimers on $(2p + 1) \times (2q + 1)$ lattices. *Physical Review E*, 73(1):016106, 2006.
- [98] V. E. Korepin. *Quantum inverse scattering method and correlation functions*. Cambridge university press, 1997.
- [99] I. A. Kovács, E. M. Elçi, M. Weigel, and F. Iglói. Corner contribution to cluster numbers in the Potts model. *Physical Review B*, 89(6):064421, 2014.
- [100] I. A. Kovács, F. Iglói, and J. Cardy. Corner contribution to percolation cluster numbers. *Physical Review B*, 86(21):214203, 2012.

- [101] W. Krauth. *Volume 13 of Oxford master series in statistical, computational, and theoretical physics.* Oxford University Press, 2006.
- [102] W. Krauth and R. Moessner. Pocket monte carlo algorithm for classical doped dimer models. *Physical Review B*, 67(6):064503, 2003.
- [103] L. Levitov. Equivalence of the dimer resonating-valence-bond problem to the quantum roughening problem. *Physical Review Letters*, 64(1):92, 1990.
- [104] E. H. Lieb. Solution of the Dimer Problem by the Transfer Matrix Method. *J. Math. Phys.*, 8(12):2339–2341, 1967.
- [105] Y. L. Loh, D.-X. Yao, and E. W. Carlson. Dimers on the triangular kagome lattice. *Physical Review B*, 78(22):224410, 2008.
- [106] L. Lovász and M. D. Plummer. *Matching theory.* Elsevier, 1986.
- [107] S. N. Majumdar and D. Dhar. Equivalence between the Abelian sandpile model and the $q \rightarrow 0$ limit of the Potts model. *Physica A: Statistical Mechanics and its Applications*, 185(1):129–145, 1992.
- [108] B. M. McCoy and T. T. Wu. *The Two-Dimensional Ising Model.* Harvard University Press, 1973.
- [109] R. Moessner and K. S. Raman. Quantum dimer models. In *Introduction to Frustrated Magnetism*, pages 437–479. Springer, 2011.
- [110] J. F. Nagle. New series-expansion method for the dimer problem. *Physical Review*, 152(1):190, 1966.
- [111] B. Nienhuis. Coulomb gas formulations of two-dimensional phase transitions. In *Phase Transitions and Critical Phenomena*, volume 11. Academic press, 1987.
- [112] B. Nienhuis, H. J. Hilhorst, and H. Blöte. Triangular sos models and cubic-crystal shapes. *Journal of Physics A: Mathematical and General*, 17(18):3559, 1984.
- [113] A. Nigro. Finite size corrections for dimers. *arXiv preprint arXiv:1208.2110*, 2012.
- [114] L. Onsager. Crystal statistics. I. A two-dimensional model with an order-disorder transition. *Physical Review*, 65(3-4):117, 1944.
- [115] S. Papanikolaou, E. Luijten, and E. Fradkin. Quantum criticality, lines of fixed points, and phase separation in doped two-dimensional quantum dimer models. *Physical Review B*, 76(13):134514, 2007.
- [116] I. Peschel. Some more results for the Ising square lattice with a corner. *Physics Letters A*, 110(6):313–315, 1985.
- [117] V. Plechko. Fermions and disorder in Ising and related models in two dimensions. *Physics of Particles and Nuclei*, 41(7):1054–1060, 2010.
- [118] V. N. Plechko. Simple solution of two-dimensional Ising model on a torus in terms of Grassmann integrals. *Theoretical and Mathematical Physics*, 64(1):748–756, 1985.
- [119] V. N. Plechko. Grassman path-integral solution for a class of triangular type decorated Ising models. *Physica A: Statistical and Theoretical Physics*, 152(1-2):51 – 97, 1988.
- [120] V. S. Poghosyan, V. B. Priezzhev, and P. Ruelle. Return probability for the loop-erased random walk and mean height in the abelian sandpile model: a proof. *Journal of Statistical Mechanics: Theory and Experiment*, 2011(10):P10004, 2011.

- [121] G. Pólya. Aufgabe 424. *Arch. Math. Phys*, 20(3):271, 1913.
- [122] A. M. Polyakov. *Gauge fields and strings*, volume 3 in Contemporary Concepts in Physics. Harwood Academic Publishers, 1987.
- [123] V. B. Priezzhev and P. Ruelle. Boundary monomers in the dimer model. *Physical Review E*, 77(6):061126, 2008.
- [124] V. Privman. *Finite-size scaling theory*, volume 1. Singapore: World Scientific, 1990.
- [125] J. Rasmussen and P. Ruelle. Refined conformal spectra in the dimer model. *Journal of Statistical Mechanics: Theory and Experiment*, 2012(10):P10002, 2012.
- [126] T. Regge and R. Zecchina. Combinatorial and topological approach to the 3d ising model. *Journal of Physics A: Mathematical and General*, 33(4):741, 2000.
- [127] D. S. Rokhsar and S. A. Kivelson. Superconductivity and the quantum hard-core dimer gas. *Physical Review Letters*, 61(20):2376, 1988.
- [128] S. Samuel. The use of anticommuting variable integrals in statistical mechanics. I. The computation of partition functions. *Journal of Mathematical Physics*, 21(12):2806–2814, 1980.
- [129] S. Samuel. The use of anticommuting variable integrals in statistical mechanics. III. Unsolved models. *Journal of Mathematical Physics*, 21(12):2820–2833, 1980.
- [130] J.-M. Stéphan. Emptiness formation probability, toeplitz determinants, and conformal field theory. *Journal of Statistical Mechanics: Theory and Experiment*, 2014(5):P05010, 2014.
- [131] J.-M. Stéphan and J. Dubail. Logarithmic corrections to the free energy from sharp corners with angle 2π . *Journal of Statistical Mechanics: Theory and Experiment*, 2013(09):P09002, 2013.
- [132] J.-M. Stéphan, G. Misguich, and V. Pasquier. Phase transition in the Rényi-Shannon entropy of Luttinger liquids. *Physical Review B*, 84(19):195128, 2011.
- [133] J.-M. Stéphan, G. Misguich, and V. Pasquier. Rényi entanglement entropies in quantum dimer models: from criticality to topological order. *Journal of Statistical Mechanics: Theory and Experiment*, 2012(02):P02003, 2012.
- [134] H. N. V. Temperley. *Combinatorics: Proceedings of the British Combinatorial Conference 1973. 202-204*. Cambridge Univ. Press. Mathematical Reviews (MathSciNet): MR345829, 1974.
- [135] H. N. V. Temperley and M. E. Fisher. Dimer problem in statistical mechanics-an exact result. *Philos. Mag.*, 6(68):1061–1063, 1961.
- [136] W.-J. Tzeng and F. Y. Wu. Dimers on a simple-quartic net with a vacancy. *Journal of Statistical Physics*, 110(3-6):671–689, 2003.
- [137] E. Vernier and J. L. Jacobsen. Corner free energies and boundary effects for Ising, Potts and fully packed loop models on the square and triangular lattices. *Journal of Physics A: Mathematical and Theoretical*, 45(4):045003, 2012.
- [138] D. Vukičević. Applications of perfect matchings in chemistry. In *Structural Analysis of Complex Networks*, page 463. Springer, 2010.
- [139] D. Vukičević. Applications of perfect matchings in chemistry. In *Structural Analysis of Complex Networks*, pages 463–482. Springer, 2011.

- [140] F. Wang and F. Y. Wu. Exact solution of close-packed dimers on the Kagomé lattice. *Physical Review E*, 75(4):040105, 2007.
- [141] F. Wang and F. Y. Wu. Dimers on the Kagomé lattice II: Correlations and the Grassmannian approach. *Physica A: Statistical Mechanics and its Applications*, 387(16):4157–4162, 2008.
- [142] F. W. Wu. Ising model with four-spin interactions. *Physical Review B*, 4(7):2312–2314, 1971.
- [143] F. Y. Wu. Dimers on two-dimensional lattices. *International Journal of Modern Physics B*, 20(32):5357–5371, 2006.
- [144] F. Y. Wu. Pfaffian solution of a dimer-monomer problem: Single monomer on the boundary. *Physical Review E*, 74:020104(R), Aug 2006. Erratum-ibid. **74**, 039907 (2006).
- [145] F. Y. Wu, W.-J. Tzeng, and N. S. Izmailian. Exact solution of a monomer-dimer problem: A single boundary monomer on a nonbipartite lattice. *Physical Review E*, 83(1):011106, 2011.
- [146] F. Y. Wu and F. Wang. Dimers on the kagome lattice I: Finite lattices. *Physica A: Statistical Mechanics and its Applications*, 387(16):4148–4156, 2008.
- [147] W. Yan, Y.-N. Yeh, and F. Zhang. Dimer problem on the cylinder and torus. *Physica A: Statistical Mechanics and its Applications*, 387(24):6069–6078, 2008.
- [148] Z. Zhang, Y. Sheng, and Q. Jiang. Monomer–dimer model on a scale-free small-world network. *Physica A: Statistical Mechanics and its Applications*, 391(3):828–833, 2012.
- [149] W. Zheng and S. Sachdev. Sine-Gordon theory of the non-Néel phase of two-dimensional quantum anti-ferromagnets. *Physical Review B*, 40(4):2704, 1989.